Chapter 3

High-Order Boundary Perturbation Methods

Oscar P. Bruno and Fernando Reitich

3.1 Introduction

Perturbation theory is among the most useful and successful analytical tools in applied mathematics. Countless examples of enlightening perturbation analyses have been performed for a wide variety of models in areas ranging from fluid, solid, and quantum mechanics to chemical kinetics and physiology. The field of electromagnetic and acoustic wave propagation is certainly no exception. Many studies of these processes have been based on perturbative calculations where the role of the variation parameter has been played by the wavelength of radiation, material constants, or geometric characteristics. It is this latter instance of geometric perturbations in problems of wave propagation that we shall review in the present chapter.

Use of geometric perturbation theory is advantageous in the treatment of configurations which, however complex, can be viewed as deviations from simpler ones—those for which solutions are known or can be obtained easily. Many uses of such methods exist, including, among others, applications to optics, oceanic and terrain scattering, SAR imaging and remote sensing, and diffraction from ablated, eroded, or deformed objects; see, e.g., [47, 52, 56, 59, 62]. The analysis of the scattering processes involved in such applications poses challenging computational problems that require resolution of the interplay between highly oscillatory waves and interfaces. In the case of oceanic scattering, for instance, nonlinear water wave interactions and capillarity effects give rise to highly oscillatory modulated wave trains that are responsible for the most substantial portions of the scattering returns [35]. Similarly, diffraction gratings owe their remarkable optical proper-

ties to their submicron features, which are designed to resonate with the incident radiation [40].

The mathematical complexities associated with these problems have historically been tackled by a variety of numerical algorithms, including methods based on integral equations, differential formalisms, Rayleigh expansions, and finite differences or finite elements. These methods can consistently provide accuracies of the order of 1% of the incident energy [38]. Classical uses of perturbation theory in these contexts have been limited to low-order methods which provide similar accuracies for problems containing small deviations. The new uses of perturbation theory that we review in this chapter, on the other hand, rely on expansions of very high order in powers of a deviation parameter, denoted here by δ, and techniques of analytic continuation in the complex δ-plane. Specifically, Taylor series for the field quantities are obtained through differentiation of the Maxwell system with respect to δ. The possible (and common) divergence of the resulting series is handled through resummation techniques that exploit the analytic structure of the solution.

The resulting algorithms can resolve scattering returns with accuracies that are several orders of magnitude better than those given by classical methods. Such accuracies can play an important role in applications. For instance, the fine resolution provided by our algorithms has recently helped settle a longstanding controversy relating to polarized back-scattering returns from rough surfaces, which amount to very small fractions of the incident energy [55].

The advantages of the use of boundary perturbation methods for calculating scattering cross sections in problems of electromagnetic and acoustic wave propagation have been recognized for several decades, since the first-order calculation of Rayleigh [50]. Besides the simplicity of their implementations, perturbation approaches generally lead, quite efficiently, to very accurate results in their domain of applicability. Indeed, it was these characteristics that prompted a number of investigations in the last 30 years, mainly in the area of scattering by corrugated surfaces, and which resulted in a variety of low-order theories [1, 2, 25, 26, 32, 44, 62]. These, of course, are limited to fairly small departures from an exactly solvable geometry, and in particular, they cannot be applied to scatterers in the resonance regime, where the wavelength is comparable to a characteristic length of the scatterer [39, 57]. In an attempt to overcome this limitation, a high-order method was proposed by Lopez, Yndurain, and Garcia [36] in the context of atom scattering from crystal surfaces and later extended to the reflection of sonic and electromagnetic waves by a number of authors [22, 23, 24, 27, 37, 53, 64]. Interestingly, these advances led to an animated debate among researchers in the area regarding the validity of series expansions in a surface-roughness parameter. In fact, even though the higher order methods did apparently extend the domain of applicability of the perturbative approach in some cases, their convergence properties remained a mystery.

This was due, in part, to the lack of understanding of the changes in the fields upon boundary variations. For instance, Lopez, Yndurain, and Garcia assumed that the field scattered by a sinusoidal surface presented a singularity at a real (and negative) value of the surface height [36, p. 972]. Greffet et al. [22, 23, 24], on the other hand, have argued that the series expansions are restricted to the do-

main of validity of the well-known Rayleigh hypothesis [38] (see also section 3.2.2) and offered this as an explanation for the limitations in the amplitudes of the perturbations for which acceptable convergence was observed. Jackson, Winebrenner, and Ishimaru presented a different view when they suggested that such series may constitute "an asymptotic expansion, valid in the limit as the roughness goes to zero" [27, p. 968]. Actually, a related conjecture had been previously advanced by Uretsky [58] in the wake of a controversial paper by Meecham [42]. Indeed, although Meecham's approach was never implemented numerically, he was perhaps the first to suggest a series representation in powers of the surface roughness. Uretsky objected to Meecham's approach and, in connection with series expansions, wrote that "it is argued that there is no circle of convergence around the origin..." [58, p. 411]. Based on the fact that the kernels in every term of the Neumann series contain branch point singularities in the perturbation variable, he went on to claim that "these considerations suggest, in fact, that the solution for the sinusoidal surface does not continue analytically to the solution for a flat surface and that we must be wary of power-series expansions in any of the parameters of the problem."

It was only a few years ago that the controversy was finally resolved when we established [7] that electromagnetic and acoustic fields *do vary analytically* with respect to variations of a scattering surface and that, in fact, *no singularities* are present for real values of the perturbation parameter (see section 3.3). Our approach relied on a potential-theoretic formulation of the mathematical problem in a *holomorphic framework* which allowed us to show, in connection with Uretsky's objection, that in spite of the occurrence of Hankel functions and associated logarithmic branch points in the iterated integrals of the Neumann series, *the integrals themselves do not contain such singularities*. In the case of analytic surfaces, these results and their nontrivial extensions to three dimensions [6] guarantee the *joint* analyticity of the fields in the spatial and parameter variables. This is to be contrasted with the classical analyticity results of Calderón [14] and Coifman, MacIntosh, and Meyer [16], which relate only to the parametric dependence and which *do not* ensure the combined holomorphic regularity. Our search for such a result, on the other hand, was motivated by the need to rigorously justify the successive differentiation of the boundary conditions of the field with respect to the perturbation parameter at the varying interface. Indeed, such differentiations result in formulas that allow for the recursive calculation of the series expansion of the fields through the solution of a sequence of scattering problems on the unperturbed geometry and that could therefore be made into the basis of a numerical algorithm (see section 3.3.2).

Besides the independent interest of our theoretical results, they also provided an explanation for the (limited) performance that numerical algorithms based on boundary variations had presented until then [22, 23, 24, 27, 36, 37, 53, 64]. Indeed, we showed that in general these limitations were related to the smallness of the radius of convergence of the perturbation series, which prevented its use in many cases of practical importance, such as in the study of highly modulated diffractive gratings. More importantly, our theory also suggested possible means to enlarge the domain of applicability of such methods. In fact, it follows from our results that in the case of (two- or three-dimensional) periodic gratings, for instance, the

scattered fields can be extended analytically to *a whole neighborhood of the real line in the complex plane of the roughness parameter*. This observation, in turn, implies that the restrictions on the convergence of the Taylor series are solely due to an unfavorable arrangement of the singularities of the fields as functions of such parameters. We therefore conjectured that their suitable rearrangement could allow for the analytic continuation of the series beyond its disk of convergence. And, in this regard, we subsequently established that such continuations may, in fact, be accurately and effectively performed through classical Padé approximation [3] or through our own summation mechanism based on conformal transformations [8, 11] (see section 3.4).

The purpose of this chapter is to present a detailed account of our high-order boundary perturbation theory and of the outcome of the resulting numerical codes. As we shall see, the capabilities of these algorithms extend well beyond those of classical perturbation procedures, and in fact they may provide, in many cases, results of an accuracy unparalleled by that given by other methods. Most of the results we present here have appeared in our papers [7, 8, 9, 10, 11, 12, 13] (an exception are those of section 3.5.3 on resonant mode calculations, which are the subject of ongoing investigations). We have attempted, however, to make this chapter self-contained, and in this spirit, our discussion begins in the following section with a number of preliminary remarks on Maxwell's equations, eigenfunction expansions (separation of variables), and far-field representations. Subsequently, in section 3.3, we present a precise description of our theoretical results on analyticity of scattered fields and of the derivation of the recursion associated with the calculation of their Taylor series representations. As we said, the resulting series may only converge in a limited regime but, as we now know, it can be continued analytically beyond its domain of convergence. Knowledge of the full Taylor series of course completely determines its analytic continuation; numerically stable and efficient methods for the calculation of analytic extensions of power series are presented in section 3.4. Finally, in section 3.5 we present numerical results for a variety of two- and three-dimensional scattering configurations, and we discuss some recent results extending our theory to evaluation of cavity eigenvalues.

3.2 Preliminaries

3.2.1 Maxwell's Equations

Consider a scattering configuration in which space is divided into two regions Ω^+ and Ω^- containing two different materials, such as air and a metal, of respective permittivities ϵ^+ and ϵ^-. The permeability of both materials is assumed to equal μ_0, the permeability of vacuum. In the cases we consider, the region Ω^+ is of infinite extent; the scatterer Ω^-, on the other hand, may be bounded or unbounded.

We wish to determine the pattern of diffraction that occurs when an electromagnetic plane wave

$$\vec{E}^i = \vec{A}e^{i(\alpha x_1+\beta x_2-\gamma x_3-i\omega t)},$$
$$\vec{H}^i = \vec{B}e^{i(\alpha x_1+\beta x_2-\gamma x_3-i\omega t)}$$

impinges upon Ω^-. Here, denoting by $\vec{k} = (\alpha, \beta, -\gamma)$ the wavevector, we have

$$\vec{A} \cdot \vec{k} = 0 \text{ and } \vec{B} = \frac{1}{\omega\mu_0}\vec{k} \times \vec{A}.$$

Dropping the factor $e^{-i\omega t}$, the time-harmonic Maxwell equations for the total fields read

$$\begin{aligned} \nabla \times \vec{E} &= i\omega\mu_0\vec{H}, \quad \nabla \cdot \vec{E} = 0, \\ \nabla \times \vec{H} &= -i\omega\epsilon\vec{E}, \quad \nabla \cdot \vec{H} = 0. \end{aligned} \tag{3.1}$$

In particular, the electromagnetic field

$$v = (\vec{E}, \vec{H})$$

satisfies the Helmholtz equations

$$\Delta v + (k^{\pm})^2 v = 0 \text{ in } \Omega^{\pm}, \tag{3.2}$$

where $k^{\pm} = \omega\sqrt{\mu_0\epsilon^{\pm}}$. The total electric and magnetic fields are given by

$$\begin{aligned} \vec{E} = \vec{E}^{out} = \vec{E}^{i} + \vec{E}^{+}, \quad \vec{H} = \vec{H}^{out} = \vec{H}^{i} + \vec{H}^{+} \text{ in } \Omega^{+} \text{ and} \\ \vec{E} = \vec{E}^{in} = \vec{E}^{-}, \quad \vec{H} = \vec{H}^{in} = \vec{H}^{-} \text{ in } \Omega^{-}, \end{aligned}$$

where $(\vec{E}^{+}, \vec{H}^{+})$ and $(\vec{E}^{-}, \vec{H}^{-})$ are the reflected and refracted fields, respectively. At the interface

$$\Gamma = \partial\Omega^{+} = \partial\Omega^{-},$$

the field satisfies the transmission conditions

$$n \times (\vec{E}^{out} - \vec{E}^{in}) = 0, \quad n \times (\vec{H}^{out} - \vec{H}^{in}) = 0 \text{ on } \Gamma, \tag{3.3}$$

where n is normal to Γ. In case the region Ω^- is filled by a perfect conductor, the refracted fields vanish and the boundary conditions reduce to

$$n \times \vec{E}^{out} = n \times (\vec{E}^{i} + \vec{E}^{+}) = 0 \text{ on } \Gamma. \tag{3.4}$$

Finally, the field satisfies conditions of radiation at infinity, expressing the outgoing character of the scattered waves, which can be stated either in terms of the eigenfunction expansions of section 3.2.2, or, alternatively, in terms of the decay of the field at infinity; see, e.g., [4, 29, 48].

In the two-dimensional case in which Γ and the fields $\vec{E}$, $\vec{H}$ are independent of x_2 (and $\beta = 0$), the system of equations (3.1), (3.3) (or (3.1), (3.4)) can be reduced to a pair of decoupled equations for two scalar unknowns [38]. Indeed, the functions $u_1(x_1, x_3)$ and $u_2(x_1, x_3)$ equal to the transverse components E_{x_2} (field transverse electric, TE) and H_{x_2} (field transverse magnetic, TM), which satisfy (3.2), completely determine the electromagnetic field through (3.1). The boundary

conditions (3.3), (3.4) can be translated into appropriate boundary conditions for the unknowns u_i. When Ω^- contains a perfect conductor, we have

$$u_1 = -e^{i\alpha x_1 - i\gamma x_3} \quad \text{and}$$

$$\frac{\partial u_2}{\partial n} = -\frac{\partial}{\partial n}\left(e^{i\alpha x_1 - i\gamma x_3}\right) \text{ on } \Gamma.$$

When Ω^- contains a finitely conducting metal or dielectric u_1 satisfies the transmission conditions

$$u_1^+ - u_1^- = -e^{i\alpha x_1 - i\gamma x_3} \quad \text{and}$$
$$\frac{\partial u_1^+}{\partial n} - \frac{\partial u_1^-}{\partial n} = -\frac{\partial}{\partial n}\left(e^{i\alpha x_1 - i\gamma x_3}\right) \quad \text{on } \Gamma,$$

while u_2 satisfies

$$u_2^+ - u_2^- = -e^{i\alpha x_1 - i\gamma x_3} \quad \text{and}$$
$$\frac{\partial u_2^+}{\partial n} - \left(\frac{k^+}{k^-}\right)^2 \frac{\partial u_2^-}{\partial n} = -\frac{\partial}{\partial n}\left(e^{i\alpha x_1 - i\gamma x_3}\right) \text{ on } \Gamma.$$

3.2.2 Eigenfunction Expansions

In addition to Taylor series, our analytic approach is based on the series expansions of the electromagnetic field which result from separation of variables. Such expansions are most frequently found in solutions associated with simple objects such as a circle, a sphere, or a semispace. This is in part due to the fact that, for such simple scatterers, the functions resulting from restriction of the separated solutions to the scattering boundaries form a complete orthonormal system, and thus boundary conditions can easily be accounted for by means of Fourier analysis.

It is interesting to note, however, that expansions in series of separated variables may be useful even when their restrictions to the boundary of the scatterer do not form an orthogonal system. The first occurrence of an approach of this type can be found in the work of Rayleigh [50]. After evaluating such expansions at the scattering boundaries, Rayleigh used appropriate approximations and found first-order corrections to the scattered field for geometries that result from small perturbations from an exactly solvable one. With the advent of computers attempts were made to extend Rayleigh's approach of evaluating series expansions at the boundary of the obstacles to general scattering solvers which do not assume small departures from an exact geometry. These attempts did not succeed since, indeed, the series may not converge at the obstacle boundaries; that is, *Rayleigh's hypothesis* may not be satisfied. This fact was first established by Petit and Cadilhac [49] by consideration of a sinusoidal corrugation on a plane.

Our method is not unrelated to Rayleigh's hypothesis. In fact, we established [7] the convergence of the eigenfunction expansions throughout the boundary for sufficiently small but otherwise arbitrary (analytic) perturbations of the exactly solvable

geometry. Whereas these "sufficiently small" perturbations for which Rayleigh's hypothesis can be used may be too small, they are certainly sufficient to allow for calculation of derivatives of any order with respect to boundary perturbations. Extension to the large perturbations that appear in practice can then be achieved by means of analytic continuation (cf. section 3.4).

The series expansions obtained from separation of variables are well known. For example, a solution to the two-dimensional Helmholtz equation outside a circular cylinder is given, in polar coordinates, by an expansion of the form

$$u(\rho,\theta) = \sum_{r=-\infty}^{\infty} B_r (-i)^r H_r^{(1)}(k\rho) e^{ir\theta}, \tag{3.5}$$

where $H_r^{(1)}$ denotes the first Hankel function of order r. The principle of conservation of energy can be given a simple form in terms of the amplitudes B_r in this expansion. Indeed, any solution u to a scattering problem from a perfectly conducting obstacle *of any shape* admits a representation (3.5) outside a cylinder containing the scatterer, and we have

$$\sum_r |B_r|^2 + \mathrm{Re}\left(\sum_r B_r\right) = 0. \tag{3.6}$$

Relation (3.6), which holds independently of whether or not the series (3.5) converges at the boundary of the obstacle, can be made into a useful estimator for errors in the numerical calculation of the fields; see section 3.5.

For a solution in three-dimensional space and outside a sphere we have

$$E^+(R,\theta,\phi) = \sum_{r=0}^{\infty} \sum_{s=-r}^{r} \vec{B}_{rs} h_r^{(1)}(kR) P_r^s(\cos(\theta)) e^{is\phi},$$

where (R,θ,ϕ) are spherical coordinates, P_r^s are the Legendre functions of the first kind, and $h_r^{(1)}$ are the first spherical Hankel functions [29].

Finally, let us consider scatterers that are given by a biperiodic corrugation of a plane

$$\Omega^- = \{x_3 < f(x_1, x_2)\}, \tag{3.7}$$

where f is a biperiodic function of periods d_1 and d_2 in the variables x_1 and x_2, respectively. These configurations arise naturally in optics applications in the form of diffraction gratings designed, for instance, to alter (reflect, absorb) incident light at specific wavelengths. In this case, the periodicity of the structure implies that the fields must be (α,β) quasi-periodic; i.e., they must verify equations of the form

$$v(x_1+d_1,x_2,x_3) = e^{i\alpha d_1} v(x_1,x_2,x_3) \ \text{ and } \ v(x_1,x_2+d_2,x_3) = e^{i\beta d_2} v(x_1,x_2,x_3).$$

Then, separation of variables leads to expansions of the form

$$\vec{E}^{\pm} = \sum_{r=-\infty}^{\infty} \sum_{s=-\infty}^{\infty} \vec{B}_{r,s}^{\pm} e^{i\alpha_r x_1 + i\beta_s x_2 \pm i\gamma_{r,s}^{\pm} x_3}.$$

The expansion for $\vec{E}^+$ (respectively, $\vec{E}^-$) converges to the field in the region $\{x_3 > \max(f(x_1, x_2))\}$ (respectively, $\{x_3 < \min(f(x_1, x_2))\}$). Here we have put

$$\alpha_r = \alpha + rK_1, \quad \beta_s = \beta + sK_2, \quad \alpha_r^2 + \beta_s^2 + (\gamma_{r,s}^{\pm})^2 = (k^{\pm})^2, \tag{3.8}$$

where $\gamma_{r,s}^{\pm}$ is determined by $\mathrm{Im}(\gamma_{r,s}^{\pm}) > 0$ or $\gamma_{r,s}^{\pm} \geq 0$,

$$(k^{\pm})^2 = \omega^2 \epsilon^{\pm} \mu_0,$$

and

$$K_1 = \frac{2\pi}{d_1}, \quad K_2 = \frac{2\pi}{d_2}.$$

It is clear from (3.8) that only a finite number of modes propagate away from the grating, since the remaining modes decay exponentially. The main quantities of interest here are the *grating efficiencies*

$$e_{r,s}^{\pm} = \frac{|B_{r,s}^{\pm}|^2 \gamma_{r,s}^{\pm}}{\gamma_{0,0}^{+}}$$

for the finitely many propagating modes, i.e., the modes (r, s) such that $\gamma_{r,s}^{\pm}$ is real. The principle of conservation of energy can be stated as follows: if we let $U^{\pm}$ denote the set of indices corresponding to the nonevanescent modes in $\Omega^{\pm}$, then

$$\sum_{(r,s)\in U^+} e_{r,s}^{+} + \sum_{(r,s)\in U^-} e_{r,s}^{-} = 1, \tag{3.9}$$

provided the dielectric constants ϵ^+ and ϵ^- are real.

In the two-dimensional case we shall consider gratings of the form

$$\Omega^- = \{x_3 < f(x_1)\},$$

for which the expansion above reduces to

$$u^{\pm} = \sum_{r=-\infty}^{\infty} B_r^{\pm} e^{i\alpha_r x_1 \pm \gamma_r^{\pm} x_3}. \tag{3.10}$$

The principle of conservation of energy now reads

$$\sum_{r\in U^+} e_r^{+} + \sum_{r\in U^-} e_r^{-} = 1, \tag{3.11}$$

where the efficiencies are now given by $e_r^{\pm} = \gamma_r^{+} |B_r^{\pm}|^2 / \gamma_0^{+}$.

3.3 Analyticity and Taylor Coefficients

3.3.1 Overview

As we said, our algorithms are based on a theorem of analyticity of the electromagnetic field with respect to boundary variations [7] (see also [6]). To describe our

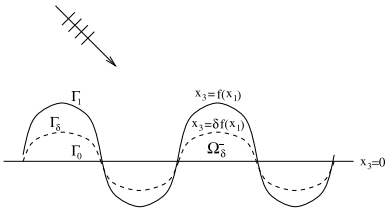

Figure 3.1: The geometry.

results assume Ω_δ^- is a family of scatterers, one for each value of the real parameter δ; see, e.g., Figure 3.1 and equation (3.14) below. Further, assume that the boundaries Γ_δ of these obstacles admit a parameterization

$$\vec{r} = H(s, \delta), \tag{3.12}$$

where the function H is jointly analytic in the spatial parameter s ($s = (s_1, s_2)$ for two-dimensional scattering interfaces) and the perturbation parameter δ. Our theorems state that both the values $v = v(\vec{r}, \delta)$ of the electromagnetic field at a fixed point in space as well as the values at a point *on the varying boundary* depend analytically on the boundary variations. More precisely, if $\vec{r}$ is a point in space away from Γ_δ and $\vec{r}_\delta \in \Gamma_\delta$ is a point on the interface which varies analytically with δ, then $v(\vec{r}, \delta)$ is jointly analytic in $(\vec{r}, \delta)$, and $v(\vec{r}_\delta, \delta)$ is an analytic function of δ for all real values of δ for which the surface (3.12) does not self-intersect.

It follows from these theorems that the field can be expanded in a series in powers of δ,

$$v^\pm(\vec{r}, \delta) = \sum_{n=0}^{\infty} v_n^\pm(\vec{r})\delta^n, \tag{3.13}$$

which converges for δ small enough. The vector field $v_n^\pm$ satisfies Maxwell's equations (3.1) as well as conditions of radiation at infinity. They also satisfy boundary conditions on $\Gamma_0 = \Gamma_\delta|_{\delta=0}$, which can be obtained by differentiation, as we show below. Such differentiations and use of the chain rule are permissible, as it follows from the analyticity theorems mentioned above and related extension theorems [6, 7]. The solution of the boundary value problems for the v_n's then easily leads to a numerical algorithm for the calculation of the scattered field.

3.3.2 Recursive Formulas

In this section we derive the recursive formulas that allow for the successive calculation of the coefficient functions $v_n^\pm$ in (3.13). The general validity of such formulas for arbitrary scattering configurations follows from the results quoted above. On the other hand, the most convenient form of the recursion for numerical implementation does, of course, depend on the geometric arrangements of interest. For instance, while Cartesian coordinates are best suited for calculations on diffraction gratings when these are viewed as modulations of a plane, polar or spherical coordinates

constitute the clear choice when dealing with bounded scatterers as perturbations of circular cylinders and spheres, respectively. In every case these formulas, together with appropriate mechanisms of analytic continuation (see section 3.4), will form the basis of our numerical approach.

Let us first consider the simplest case of a family of two-dimensional perfectly conducting and d-periodic diffraction gratings

$$\Omega_\delta^- = \{x_3 < \delta f(x_1)\}, \tag{3.14}$$

for which the far-field eigenfunction expansions take the form (cf. (3.10))

$$u(x_1, x_3, \delta) = u^+(x_1, x_3, \delta) = \sum_{r=-\infty}^{\infty} B_r(\delta) e^{i\alpha_r x_1 + \gamma_r x_3} \tag{3.15}$$

with

$$\alpha_r = \alpha + \frac{2\pi}{d} r \quad \text{and} \quad \alpha_r^2 + \gamma_r^2 = k^2.$$

From section 3.3.1 we have an expansion

$$u(x_1, x_3, \delta) = \sum_{n=0}^{\infty} u_n(x_1, x_3)\delta^n,$$

which converges for sufficiently small values of δ. The functions

$$u_n(x_1, x_3) = \frac{1}{n!} \frac{\partial^n u}{\partial \delta^n}(x_1, x_3, 0)$$

satisfy the Helmholtz equation

$$\Delta u_n + k^2 u_n = 0 \text{ in } \{\, (x_1, x_3) \,:\, x_3 > 0 \,\} \tag{3.16}$$

and conditions of radiation at infinity. Thus, an expansion analogous to (3.15) holds for u_n itself,

$$u_n(x_1, x_3) = \sum_{r=-\infty}^{\infty} d_{n,r} e^{i\alpha_r x_1 + i\gamma_r x_3}. \tag{3.17}$$

We clearly have

$$d_{n,r} = \frac{1}{n!} \frac{d^n B_r}{d\delta^n}\bigg|_{\delta=0},$$

so that the amplitudes of the various modes are given by the Taylor series

$$B_r(\delta) = \sum_{n=0}^{\infty} d_{n,r}\delta^n. \tag{3.18}$$

Our approach is based on evaluation of the Taylor series (3.18), whose coefficients $d_{n,r}$ can be obtained recursively. Such recursive formulas follow from the *explicit* successive solution of (3.16) subject to appropriate boundary conditions on the plane $x_3 = 0$. These conditions can be easily derived from the values of the field at the scattering surfaces which, in this case, may be written in the form

$$u(x_1, \delta f(x_1), \delta) = -e^{i\alpha x_1 - i\gamma\delta f(x_1)}.$$

Indeed, differentiation of this relation at $\delta = 0$ simply gives

$$u_n(x_1, 0) = -\frac{(-i\gamma f(x_1))^n}{n!} e^{i\alpha x_1} - \sum_{l=0}^{n-1} \frac{f(x_1)^{n-l}}{(n-l)!} \frac{\partial^{n-l} u_l}{\partial x_3^{n-l}}(x_1, 0). \tag{3.19}$$

Now, let the Fourier series of the function $f(x_1)$ be given by

$$f(x_1) = \sum_{r=-F}^{F} C_{1,r} e^{i2\pi r x_1/d}$$

with either finite or infinite F. Then, substitution in (3.19) of u_l $(0 \le l \le n)$ and their x_3-derivatives as calculated from (3.17) permits us to find all the coefficients $d_{n,r}$ in terms of the coefficients $d_{k,r}$ with $k < n$ and the Fourier series coefficients $C_{l,r}$ of the function $f(x_1)^l/l!$:

$$\frac{f(x_1)^l}{l!} = \sum_{r=-lF}^{lF} C_{l,r} e^{i2\pi r x_1/d}.$$

In fact, from (3.19) we have

$$\sum_{r=-\infty}^{\infty} d_{n,r} e^{i\alpha_r x_1} = -(-i\gamma)^n \left(\sum_{r=-nF}^{nF} C_{n,r} e^{i\alpha_r x_1} \right) - \sum_{l=0}^{n-1} \left(\sum_{s=-(n-l)F}^{(n-l)F} C_{n-l,s} e^{i2\pi s x_1/d} \right) \left(\sum_{q=-\infty}^{\infty} d_{l,q} (i\gamma_q)^{n-l} e^{i\alpha_q x_1} \right),$$

or equivalently,

$$\begin{aligned} \sum_{r=-\infty}^{\infty} d_{n,r} e^{i\alpha_r x_1} &= -\sum_{r=-nF}^{nF} (-i\gamma)^n C_{n,r} e^{i\alpha_r x_1} \\ &\quad - \sum_{l=0}^{n-1} \sum_{s=-(n-l)F}^{(n-l)F} \sum_{q=-\infty}^{\infty} C_{n-l,s} d_{l,q} (i\gamma_q)^{n-l} e^{i\alpha_{s+q} x_1} \\ &= -\sum_{r=-nF}^{nF} (-i\gamma)^n C_{n,r} e^{i\alpha_r x_1} \\ &\quad - \sum_{l=0}^{n-1} \sum_{q=-\infty}^{\infty} \sum_{r=q-(n-l)F}^{q+(n-l)F} C_{n-l,r-q} d_{l,q} (i\gamma_q)^{n-l} e^{i\alpha_r x_1}. \end{aligned}$$

Thus, we have

$$d_{n,r} = -(-i\gamma)^n C_{n,r} - \sum_{l=0}^{n-1} \sum_{q=r-(n-l)F}^{r+(n-l)F} C_{n-l,r-q}(i\gamma_q)^{n-l} d_{l,q}, \tag{3.20}$$

where, of course,

$$d_{0,0} = -1,$$

as it follows from the law of reflection onto a planar surface.

Analogous formulas can be derived for two-dimensional bounded obstacles when viewed, for instance, as perturbations of a circular cylinder or any other exactly solvable geometry. More precisely, for obstacles whose boundaries are given, in polar coordinates, by

$$\Gamma_\delta = \{(\rho, \theta) \,:\, \rho = a + \delta f(\theta)\}, \tag{3.21}$$

the recursion reads

$$\begin{aligned} d_{n,q} = &-k^n \sum_{p=q-nF}^{q+nF} C_{n,q-p}(-i)^{p-q} \frac{d^n J_p}{dz^n}(ka)/H_q^{(1)}(ka) \\ &- \sum_{l=0}^{n-1} k^{n-l} \sum_{p=q-(n-l)F}^{q+(n-l)F} d_{l,p} C_{n-l,q-p}(-i)^{p-q} \frac{d^{n-l} H_p^{(1)}}{dz^{n-l}}(ka)/H_q^{(1)}(ka), \end{aligned} \tag{3.22}$$

where again $d_{n,r}$ denotes the Taylor coefficients of the amplitudes B_r (cf. (3.18)), which are now defined through (3.5) and

$$\frac{f(\theta)^l}{l!} = \sum_{r=-lF}^{lF} C_{l,r} e^{ir\theta}.$$

In this case, the calculation is initialized by means of the relations

$$d_{0,q} = -J_q(ka)/H_q^{(1)}(ka),$$

which follow from the exact expressions for the field scattered by a circular cylinder of radius a (see [4]). For the general formulas corresponding to the vector scattering problem in three dimensions we refer the reader to [10] for details on the treatment of biperiodic gratings and to [13] for those on three-dimensional bounded scatterers.

3.3.3 Calculation of Taylor Coefficients

Recursive formulae such as (3.20) and (3.22) allow us to compute Taylor coefficients of a scattering problem to arbitrarily high orders. To demonstrate the calculation, let us take a simple case of a two-dimensional grating (3.14) with

$$f(x_1) = 2\cos(Kx_1) = e^{iKx_1} + e^{-iKx_1}, \tag{3.23}$$

for which $F = 1$, $C_{n,k} = 0$ if $n - k$ is odd, and $C_{n,k} = \frac{1}{n!}\binom{n}{\frac{n-k}{2}}$ if $n - k$ is even. Then, it is easy to see from (3.20) that the nonzero coefficients $d_{n,r}$ are

$$\begin{array}{ccccccccc} & & & & d_{0,0} = -1 & & & & \\ & & & d_{1,-1} & & d_{1,1} & & & \\ & & d_{2,-2} & & d_{2,0} & & d_{2,2} & & \\ & d_{3,-3} & & d_{3,-1} & & d_{3,1} & & d_{3,3} & \\ d_{4,-4} & & d_{4,-2} & & d_{4,0} & & d_{4,2} & & d_{4,4} \\ & & & & \text{etc.} & & & & \end{array}$$

If an Nth-order approximation to the Taylor series in (3.18) is to be computed, it is clearly unnecessary to produce *all* of the coefficients $d_{n,r}$ for $n \le N$. In fact, to compute B_0 with $N = 4$ we need only generate

$$\begin{array}{ccccc} & & d_{0,0} = -1 & & \\ & d_{1,-1} & & d_{1,1} & \\ d_{2,-2} & & d_{2,0} & & d_{2,2} \\ & d_{3,-1} & & d_{3,1} & \\ & & d_{4,0} & & \end{array} \tag{3.24}$$

Of course, in general we wish to obtain not only B_0 but a number w of amplitudes that will in turn be used to calculate the fields with a given accuracy; the arrays of derivatives must be augmented accordingly. Similar considerations apply to functions f given by an arbitrary finite Fourier series.

In practice, and in order to reduce the number of operations, one can choose to truncate the inner sum in equations such as (3.20) by setting $d_{k,q} = 0$ for $|q| > q_0$. The parameter q_0 has to be chosen judiciously. Our experiments indicate that in the case of the sinusoidal profile (3.23), no truncation is permissible (e.g., one cannot take $q_0 < 2$ in (3.24)). On the other hand, for the grating associated with the function

$$f(x_1) = 2\cos(Kx_1) + \frac{1}{5}\cos(3Kx_1), \tag{3.25}$$

the effect of the higher order harmonics generated by the second summand can be truncated. In other words, even though the actual formula (3.20) for this profile involves frequencies roughly as high as $\frac{3}{2}N + w$, one can take $q_0 = \frac{N}{2} + w$ with errors comparable to roundoff. This is related to the fact that the height-to-period ratio h/d of the first term in (3.25) is larger than the one for the second term. Thus, in the general case of a general Fourier series, q_0 should be chosen so that no truncation would occur if all but the principal terms in it (i.e., the ones with the largest h/d's) were neglected. Naturally, as the height-to-period ratio of a secondary term approaches those for the principal terms, the value of q_0 should be increased. The ultimate choice of q_0 must be made by consideration of the actual errors as measured by the defect in the energy balance, convergence, reciprocity, or other criteria.

In the case of the sinusoidal grating considered above, closed form expressions for the coefficients $C_{n,r}$ of (3.20) were found. This is, of course, not possible if

the boundary of the scatterer is given by an arbitrary function f. By appropriate truncation we may always assume that f is given by a *finite* Fourier series containing modes with orders between $-F$ and F, say; simple iterated multiplication of the series of f then yields a very stable algorithm for the calculation of $C_{n,r}$. Convergence as F is increased is then the criterion for an appropriate choice of this parameter.

Now the issue arises that calculation of the complete powers of the Fourier series of f may be prohibitively expensive in the three-dimensional cases—even when F is as small as, say, $F = 10$. It is therefore fortunate that, again, appropriate truncations can be used with errors comparable with roundoff. The procedure is very simple indeed: if the Fourier series of f^n has been computed, then all modes of order r with $|r| > q_1$ are set to zero, and the resulting series is multiplied by the series of f. The result is then taken as an approximation to f^{n+1}. Of course, the choice of the parameter q_1 depends on the particular scatterer, on F, on q_0, and on the order n of the Taylor approximation. We can assume that appropriate values of these parameters have been found when further increases in them do not lead to improvements in the numerical error.

To complete our algorithms we must now consider the question of summation of series such as (3.18). As we have said, the functions $B_r(\delta)$ are analytic in a common neighborhood of the real axis, and therefore the series in (3.18) certainly has a positive radius of convergence. It turns out that this series diverges (or converges slowly) for many cases of interest, and we thus need appropriate numerical schemes for analytic continuation in the complex δ plane. This is the subject of the following section.

3.4 Approximation of Analytic Functions

Our understanding of the problem of calculation of the electromagnetic field by means of analytic continuation can be presented at two different levels of detail. On one hand we may accurately state that Padé approximants have produced better accuracy than other approximators in all the applications of our method we have encountered. We therefore view Padé approximation, which is briefly described below, as an integral element of our algorithms. An interesting insight into the approximation problem, on the other hand, can be gained by consideration of the spectrum of singularities of the field *as a function of the perturbation parameter* δ. Indeed, singularities play a major role in the approximation problem. They determine the radius of convergence of the Taylor series and they are closely related to the speed of convergence of Padé approximants [3]. Further, the spectrum of singularities determines the conditioning in the values of the Padé approximants [11], and even partial information on such singularities may be used in some cases to produce a rather dramatic improvement in the Padé problem; a simple example of this phenomenon is presented at the end of this section. Our current knowledge of the analytic structure of the field in the δ plane is discussed in what follows.

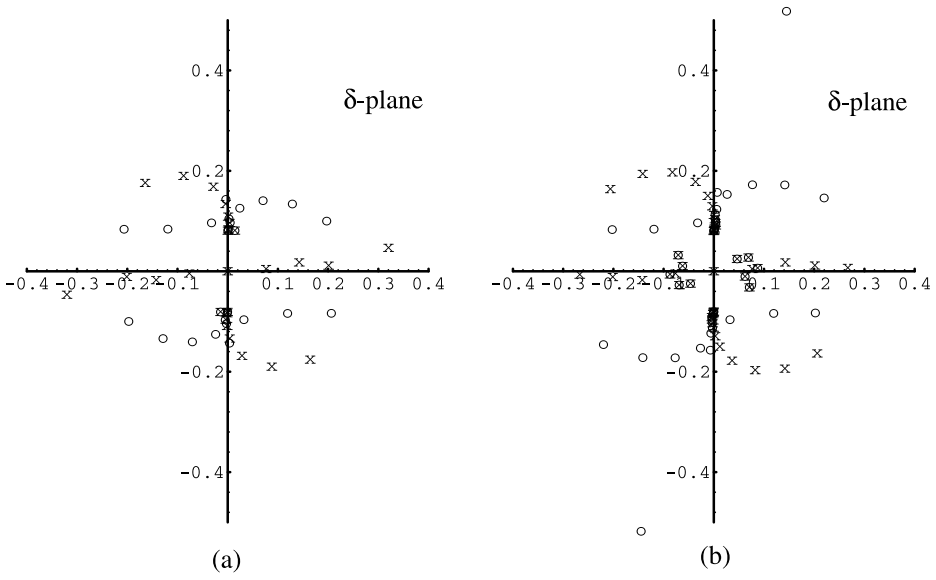

Figure 3.2: Poles (o) and zeros (x) of the Padé approximants of $B_1(\delta)$: (a) [28/28]-approximant; (b) [48/48]-approximant.

The $[L/M]$ Padé approximant of a function

$$B(\delta) = \sum_{n=0}^{\infty} d_n \delta^n \tag{3.26}$$

is defined (see [3]) as a rational function

$$[L/M] = \frac{a_0 + a_1\delta + \cdots + a_L\delta^L}{1 + b_1\delta + \cdots + b_M\delta^M}$$

whose Taylor series agrees with that of B up to order $L + M + 1$. A particular $[L/M]$ approximant may fail to exist but, generically, $[L/M]$ Padé approximants exist and are uniquely determined by L, M, and the first $L + M + 1$ coefficients of the Taylor series of B. Padé approximants have some remarkable properties of approximation of analytic functions from their Taylor series (3.26) for points far outside their radii of convergence; see, e.g., [3]. They can be calculated by first solving a set of linear equations for the denominator coefficients b_i, and then using simple formulae to compute the numerator coefficients a_i. For convergence studies and numerical calculation of Padé approximants, see [3, 5, 21].

In Figure 3.2 we show the location of the zeros of the numerators and denominators of the [28/28] and [48/48] Padé approximants to the coefficient $B_1(\delta)$ for the perfectly conducting grating with profile

$$f_\delta(x_1) = \delta(e^{i2\pi x_1} + e^{-i2\pi x_1}) = 2\delta\cos(2\pi x_1)$$

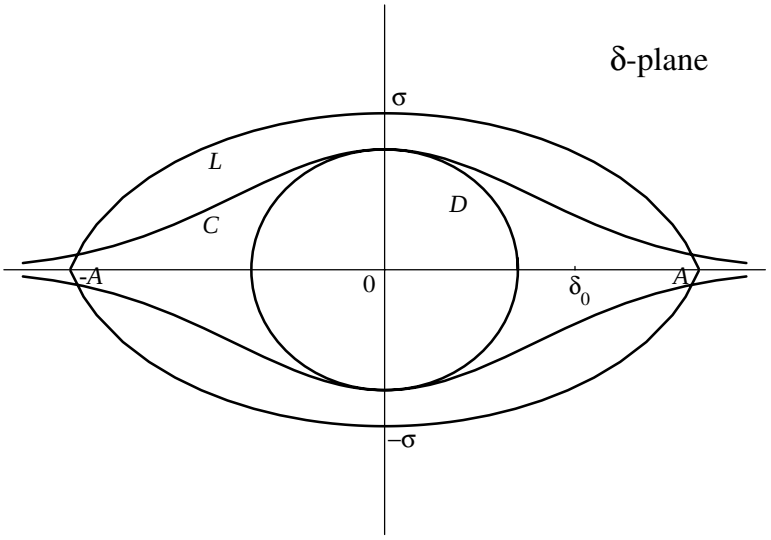

Figure 3.3: The region C of analyticity of the Rayleigh coefficients $B_r^{\pm}(\delta)$ and a lens-shaped region L that is conformally transformed onto the right half-plane via $g(\delta) = (\frac{A-\delta}{A+\delta})^{\alpha}$.

under normal incidence and with light of wavelength $\lambda = 0.4368$. In this figure, a circle (o) represents a zero of the denominator, which is a singularity of the approximant provided it is not crossed out by a corresponding zero (x) in the numerator. Very similar pictures are obtained for other amplitudes B_r and for approximants of other orders. Now, it is well known that, rather generally, the singularities of the Padé approximants approach the singularities of the function they approximate [3]. Thus, Figure 3.2 provides us with an approximation to the domain of analyticity of the diffracted fields. Note that no singularities occur on the real axis, as expected from the theoretical discussion of section 3.3.1.

A domain of analyticity C which resembles the one suggested by Figure 3.2 was proposed in [8]; see Figure 3.3. This picture led us to devise a summation mechanism based on conformal transformations that we called *enhanced convergence* [8, 11]; see also [54]. Given a function $B(\delta)$ and a complex number δ_0, the method of enhanced convergence uses conformal mappings to produce an appropriate arrangement of the singularities of B and the point δ_0, so that a truncated Taylor series can be used to calculate $B(\delta_0)$.

Suppose we wish to compute the function $B(\delta)$ at a point δ_0 which lies outside the circle of convergence D of the Taylor series of B around $\delta = 0$ (see Figure 3.3). The series is divergent at δ_0. If we consider, however, the composition of B with a conformal transformation,

$$\xi = g(\delta),$$

Table 3.1: Comparison between direct and enhanced convergence. First-order efficiency for a sinusoidal grating in TE polarization, $\delta = 0.075$.

	Direct		Enhanced	
n	e_1	ϵ	e_1	ϵ
10	0.5034545E–02	1.5E–01	0.1735547E–01	8.3E–02
15	0.1073396E–01	5.3E–02	0.1204894E–01	1.3E–05
20	0.1045474E–01	4.0E–03	0.1157684E–01	5.1E–04
25	0.1140532E–01	3.2E–03	0.1163189E–01	3.1E–05
30	0.1161950E–01	2.2E–04	0.1163870E–01	–8.4E–06
35	0.1165000E–01	1.1E–05	0.1163798E–01	–7.3E–07
40	0.1162548E–01	–3.2E–05	0.1163793E–01	–4.4E–08
45	0.1163059E–01	5.1E–05	0.1163793E–01	2.2E–08
50	0.1164204E–01	1.2E–05	0.1163793E–01	2.0E–09
55	0.1164090E–01	–1.7E–05	0.1163793E–01	–3.7E–11
60	0.1163616E–01	–4.0E–06	0.1163793E–01	–4.5E–11

Table 3.2: Comparison between direct and enhanced convergence. First-order efficiency for a sinusoidal grating in TE polarization, $\delta = 0.1$.

	Direct		Enhanced	
n	e_1	ϵ	e_1	ϵ
10	0.3897061E+00	–7.2E–01	0.4018525E+00	–4.5E–01
15	0.4713435E+01	–1.4E+01	0.1649737E+00	–7.3E–02
20	0.3635994E+01	–1.5E+01	0.1568326E+00	3.1E–02
25	0.3848452E+01	–1.2E+01	0.1687898E+00	4.8E–03
30	0.3357765E+00	–5.5E+00	0.1698172E+00	3.0E–04
35	0.1276039E+01	–2.4E+01	0.1701259E+00	–4.0E–04
40	0.4143993E+02	–2.2E+02	0.1700261E+00	–1.3E–04
45	0.1665033E+03	–1.6E+03	0.1699795E+00	1.3E–05
50	0.1406855E+04	–8.2E+03	0.1699760E+00	1.1E–05
55	0.7075471E+04	–6.9E+04	0.1699781E+00	2.5E–06
60	0.7847034E+05	–4.1E+05	0.1699792E+00	–4.8E–07

the singularities and the point $\xi_0 = g(\delta_0)$ at which the function is sought will show a different arrangement *in the ξ plane*, and ξ_0 may lie inside the circle of convergence of the composite function $B(g^{-1}(\xi))$. If so, a truncated Taylor series of the composite function can be summed to yield the value $B(\delta_0)$. Even if δ_0 lies inside the circle of convergence D, this procedure may result in improved convergence rates [8, 11]. In Tables 3.1 and 3.2, for example, we compare the convergence of the power series for $e_1(\delta) = |B_1(\delta)|^2\beta_1/\beta_0$ about $\delta = 0$ ("Direct") with that of $e_1(\xi) = |B_1(\xi)|^2\beta_1/\beta_0$ ("Enhanced") obtained by means of an appropriate conformal change of variables [8]. Again we consider the sinusoidal grating scattering problem mentioned above. We observe that even in the case $\delta = 0.075$, in which the direct series converges, the convergence is substantially enhanced by the conformal mapping. In case $\delta = 0.1$ the direct series does not converge.

The performance of this summation method depends strongly on the parameters A and σ of Figure 3.3. The optimality of a choice of these parameters can be checked through the defect ϵ in the energy relation (3.11)

$$\epsilon = 1 - \sum_{n \in U^+} e_n^+.$$

($e_n^- = 0$ here, since we are dealing with a perfectly conducting grating.) Alternatively, the optimal values of these parameters can be calculated [9] by consideration of the poles shown in Figure 3.2. The results of these calculations are in close agreement. Further, note the position of singularities closest to the origin in Figure 3.2, which implies a radius of convergence consistent with the convergence results of the direct series in Tables 3.1 and 3.2. The agreements found in these calculations constitute an important consistency check in our theory. In addition, they add substantial credibility to our view that the analytic structure in the δ plane is well approximated by representations such as that in Figure 3.2.

As we said, Padé approximation does exhibit better numerical performance than enhanced convergence; in the examples of Tables 3.1 and 3.2, for instance, Padé approximants permit us to obtain two additional significant digits [9]. Interestingly, enhanced convergence can be used to improve the performance of Padé approximation. Indeed, the theory in [11] shows that the relative arrangement of the singularities of an analytic function is closely related to the numerical conditioning of the corresponding Padé problem. Further, a conformal change of variables on a function $B(\delta)$ can lead to a dramatic improvement in this conditioning. (The Padé approximants of the functions in the transformed variables will be referred to as enhanced Padé approximants.) Since the main numerical weakness of Padé approximation is its ill conditioning, it is reasonable to expect that enhanced approximants could lead to improvement in our solutions of scattering problems. Unfortunately, we have not yet succeeded in devising a numerical implementation of these ideas in the context of scattering calculations that will meet a basic requirement of the approach, namely, the need for *accurate* values of the Taylor coefficients of the composite functions. Composition of the corresponding series, which certainly suffices in applications such as those of Tables 3.1 and 3.2, is not appropriate for the enhanced Padé application. Indeed, composition of power series leads to a loss of significant digits in the Taylor coefficients. This accuracy loss interacts with the conditioning problem of Padé approximation in such a way that no substantial improvements in the calculated values are obtained. If accurate values of the coefficients of the composite functions can be found, on the other hand, then very substantial improvements can be obtained, as shown in an example below. Thus, further improvement in the performance of our algorithms could result if an accurate method for computation of the enhanced coefficients were found.

As we said, enhanced convergence may help obtain a remarkable improvement in the performance of Padé approximation. Let us consider, for example, Table 3.3, which shows the values of the $[\frac{N}{2}/\frac{N}{2}]$ Padé and enhanced Padé approximants for the function $f(z) = \log(1+z)$; see [11] for details. This table shows that enhanced Padé approximants produce up to 13 correct digits of $\log(21)$ while ordinary Padé

Table 3.3: $[\frac{N}{2}/\frac{N}{2}]$ approximants for $\log(1+z)$.

N	z	$\log(1+z)$	Padé	Enh. Padé
20	20	3.044522437723	3.043989111079	3.043988784141
40			3.044612164211	3.044522360574
60			3.044477040660	3.044522437596
80			3.044175772366	3.044522437727
100			3.044463021924	3.044522437722
120			3.044489520809	3.044522437724
140			3.044496462919	3.044522437723
160			3.044619592662	3.044522437723
180			3.044362344599	3.044522437723
20	200	5.30330	5.03582	5.03577
40			5.32614	5.28588
60			5.17831	5.30093
80			5.08690	5.30276
100			5.16939	5.30305
120			5.18899	5.30324
140			5.19792	5.30328
160			5.70660	5.30329
180			5.13885	5.30330

fractions do not produce more than the first 4 digits. It is very remarkable, in any case, that the Padé approximation is so stable and that it produces these four digits for N up to at least $N = 180$, in spite of the tremendous ill-conditioning of the denominator problem. Table 3.3 also shows the values of both approximants at $z = 200$; again, an improvement is observed.

3.5 Applications

The difficulty associated with the numerical solution of a scattering problem depends roughly on two elements: the magnitude of the ratio P/λ of the "size" (characteristic length) of the scatterer to the wavelength on one hand, and the oscillations and/or lack of smoothness exhibited by its boundary, on the other. In short, numerical complexity arises from the need to account accurately for oscillatory behavior of fields and interfaces. In what follows we present applications of our method which test its performance in problems of various degrees of difficulty, and we compare the results of these algorithms with those given by classical methods.

As we have noted, our approach is applicable to configurations that may be viewed as perturbations from an exactly solvable geometry. Such perturbations need not be small, as may be seen from the examples that follow, and our analytic method may be considered as a rather general one. In many cases of practical importance our approach yields results that are several orders of magnitude more accurate than those given by classical methods, such as the method of moments and other algorithms based on the solution of integral equations.

3.5.1 Two-Dimensional Problems

We have tested our analytic method in a variety of problems of diffraction by gratings [9], and indeed, our method was originally intended as a grating solver. We therefore discuss applications to grating problems first. To substantiate the general applicability of our approach, we also include here an example of a calculation of the radar cross section (RCS) generated by a bounded cylindrical obstacle, and a corresponding example in three dimensions is given in section 3.5.2. In this and the following sections the error estimator ϵ is the defect in the energy balance criterion. For example, in the grating configurations ϵ is defined as the defect in the relations (3.9) and (3.11), and for two-dimensional dielectric gratings, ϵ is given by

$$\epsilon = 1 - \sum_{r \in U^+} e_r^+ - \sum_{r \in U^-} e_r^-$$

as calculated by the numerical solver. For a perfectly conducting bounded obstacle in two dimensions ϵ is defined as the relative error in the calculated value of the left-hand side of equation (3.6):

$$\epsilon = \frac{\left| \sum_r |B_r|^2 + \mathrm{Re}\left(\sum_r B_r\right) \right|}{\sum_r |B_r|^2}. \tag{3.27}$$

These defects provide an accurate measure of the relative error in the quantities of interest. Indeed, unlike other approaches, our method does not verify energy balance exactly, so that its defect is in fact a good accuracy estimator. We have verified this through convergence tests in a large number of examples; e.g., compare efficiency errors and energy defects in the results of Tables 3.1 and 3.2. Of course, the energy balance criterion is only valid in the absence of absorption. When dealing with lossy scatterers we generally turn to estimating the errors directly by means of convergence tests, as in the first application in section 3.5.2.

In our first example we consider a problem of diffraction by a sinusoidal dielectric grating (3.14) with

$$f(x_1) = 2\cos(2\pi x_1/d)$$

and period $d = 1\mu m$. (Note that the height h of the corrugations, that is, the vertical distance from the highest peak to the lowest valley, is given by $h = 4\delta$.) The grating has a refractive index $\nu_0 = 2$ and is illuminated under normal incidence with light of wavelength $\lambda = 0.83\mu m$. Table 3.4 contains results given by our algorithms for the reflected and transmitted energy R and T, which results from a unit input energy. This case was treated in [18] by means of integral equations and the method of moments; there, the authors report the following values of R and T for $h = 0.2\mu m$:

$$R = 0.117274,$$

$$T = 0.882759,$$

Table 3.4: Reflected and transmitted energies for a sinusoidal grating with index of refraction $\nu_0 = 2$, under normal incidence with a wavelength-to-period ratio $\lambda/d = 0.83$: [20/20] Padé approximants. Left: TE polarization; right: TM polarization.

h/d	R	T	ϵ	h/d	R	T	ϵ
0.00	0.111111	0.888889	−2.2E−16	0.00	0.111111	0.888889	−2.2E−16
0.10	0.114926	0.885074	0.0E+00	0.10	0.104046	0.895954	−2.2E−16
0.20	0.117282	0.882718	0.0E+00	0.20	0.086355	0.913645	0.0E+00
0.30	0.104871	0.895129	1.6E−14	0.30	0.062807	0.937193	−1.6E−12
0.40	0.080184	0.919816	9.8E−11	0.40	0.039117	0.960883	−1.1E−08
0.50	0.055902	0.944098	1.0E−07	0.50	0.025636	0.974363	−6.5E−07
0.60	0.038983	0.961015	−1.3E−06	0.60	0.023655	0.976517	1.7E−04
0.70	0.029619	0.969848	−5.3E−04	0.70	0.021333	0.982000	3.3E−03
0.80	0.024083	0.972233	−3.7E−03	0.80	0.016013	0.999951	1.6E−02

and

$$\epsilon = 1 - (T + R) = 3.3 \times 10^{-5};$$

compare the left side of Table 3.4.

As is the case here, the analytic method yields results of very good definition in most grating problems of interest. Other results for grating problems obtained by discretization of boundary integral equations include, for example, those of Van den Berg [60] and Pavageau and Bousquet [46]. These authors considered a perfectly conducting sinusoidal grating for values of h/d ranging from 0.3 to 0.56 and illuminated with light of wavelength $\lambda = 0.4368$. They report errors of the order of 10^{-5} for a ratio of 0.3 and of order 10^{-3} for ratios of 0.4 and 0.56. The corresponding errors in the analytic method are of order 10^{-12}, 10^{-8}, and 10^{-6}; similar improvements in performance over other methods have been found in calculations containing lossy gratings and nonsmooth (e.g., triangular) profiles [9]. It must be pointed out that the largest ratio $h/d = 0.56$ considered here is larger than those corresponding to gratings actually used in applications [40]. For even deeper gratings, say, ratios of 0.7 and beyond (and for this wavelength), our method in its present form rapidly breaks down due to numerical ill-conditioning, while the integral method deteriorates more slowly, and it gives results with errors of a few percent for gratings with heights as large as $h/d = 1$. As we pointed out in section 3.4, remedies for conditioning problems in our algorithms may result from a more detailed consideration of the analytic properties and singularities of the electromagnetic field; see, e.g., Table 3.3.

In our second example we study scattering by the perfectly conducting obstacle of Figure 3.4(a) (a two-dimensional bounded scatterer without symmetries) to demonstrate the wider applicability of our methods. The boundary of this obstacle is given by (3.21) with $f(\theta) = 0.125\sin(4\theta) - 0.15\sin(3\theta)$ and $\delta = 1$. Figure 3.4(b) gives the amplitude of the bistatic far field coefficient Φ for the TE polarized configuration indicated in Figure 3.4(a) with perimeter-to-wavelength ratio $P/\lambda = 20$.

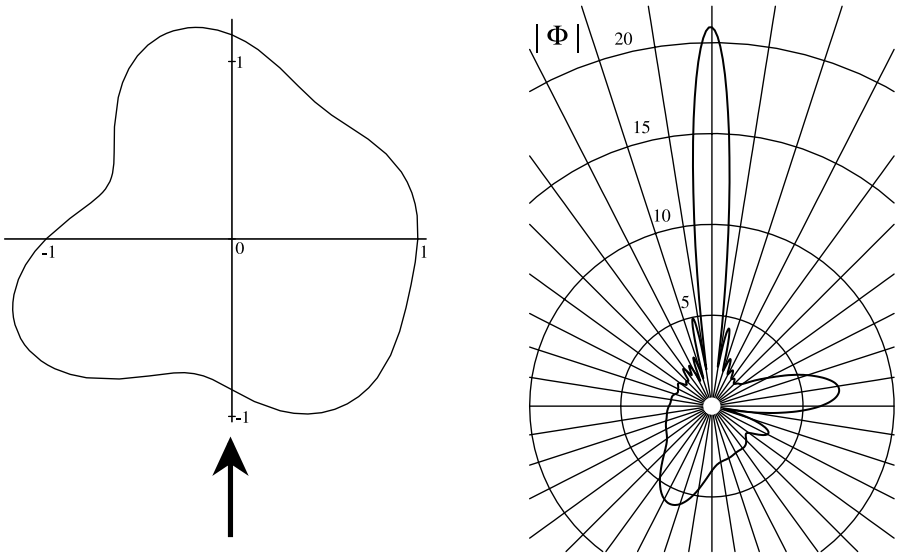

(a) (b)

Figure 3.4: (a) A two-dimensional bounded scattering configuration without symmetries, (b) the amplitude of its bistatic far-field coefficient Φ. TE polarization, $P/\lambda = 20$.

3.5.2 Three-Dimensional Problems

In this section, we present results of applications of our approach to truly three-dimensional geometries. We begin again with the case of optical diffraction gratings, where we consider the full problem of electromagnetic scattering (Maxwell's equations) off biperiodic surfaces. After a discussion of smooth (sinusoidal) metallic gratings, we turn to a challenging example of a configuration that presents edges and corners. Finally, we again demonstrate the generality of the approach by briefly recounting the outcome of our numerical methods in the case of (acoustic) scattering by three-dimensional bounded bodies.

Bisinusoidal gratings in gold have been used in the experimental and numerical studies on total absorption; see [41]. These are gratings of the form (3.7) with

$$f(x_1, x_2) = \left[\cos\left(\frac{2\pi x_1}{d_1}\right) + \cos\left(\frac{2\pi x_2}{d_2}\right)\right] \quad \text{(see Figure 3.5)};$$

note that the groove depth is again given by $h = 4\delta$. In [41] the authors treated this problem by means of the integral method of [17]; they considered gratings with depths of $h = 0.040$, $h = 0.055$, and $h = 0.070$ and with periods $d_1 = d_2$ varying from 0.60 to 0.64. In Figure 3.6 we show the results given by our algorithm for these problems. Qualitative agreement with the results in [17, 41] is observed, but some discrepancies occur. For example, in contrast with Figure 7.17 of [41], our

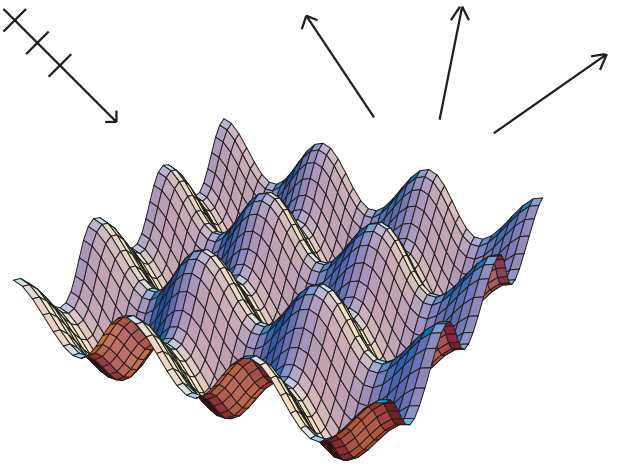

Figure 3.5: Section of a three-dimensional bisinusoidal diffraction grating.

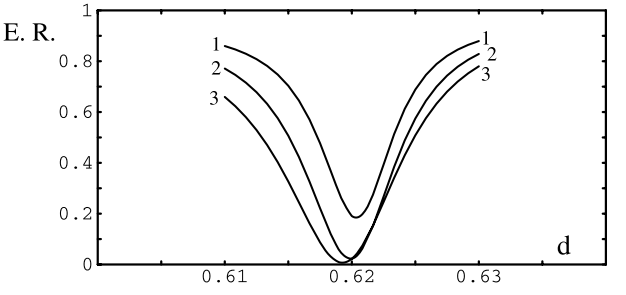

Figure 3.6: Energy reflected by the bisinusoidal grating of Figure 3.5 (in gold), with normally incident light of wavelength 0.65μm. Curve 1: $h = 0.040\mu$m; curve 2: $h = 0.055\mu$m; curve 3: $h = 0.070\mu$m: [6/6] Padé approximants.

curves 2 and 3 coincide at $d = 0.62\mu$m. This prompted us to analyze the accuracy of our results. We found that, for this range of parameters, our method yields extremely accurate results, with errors in the reflected energy ("E.R.") that are better than 10^{-14}. This can be seen in Table 3.5, which contains a convergence study for the values of the reflected energy at $d = 0.62\mu$m for the curves labeled 2 and 3 in Figure 3.6. Note that an accuracy better than eight digits is obtained by an approximation of order 13. The accuracy of the integral method in this problem ($h = 0.055$ and $h = 0.070$) has been estimated to be of the order of two digits [17]. To demonstrate the range of parameters in which our method can be applied, we include a third column in Table 3.5 showing the values of E.R. for a much deeper grating profile of height $h = 0.500\mu$m, for which $h/d = 0.806$. We see that even in this case, the results are quite accurate: the errors are of the order of 10^{-4} for a [6/6] approximant ($n = 13$) and of 10^{-6} for a [14/14] approximant ($n = 29$). (Padé approximants with $n = 15$, 19, 23, 27, and 31 are singular for this problem.)

Table 3.5: Convergence study of the reflected energy for the example in Figure 3.5 (gold). The period is fixed at 0.62μm and the wavelength at 0.65μm. $[\frac{n-1}{2}/\frac{n-1}{2}]$ Padé approximants.

n	$h = 0.055\mu$m	$h = 0.070\mu$m	$h = 0.500\mu$m
13	0.0227882361359963	0.0226057361431067	0.84146746
17	0.0227882361334883	0.0226057359874209	0.84202623
21	0.0227882361334891	0.0226057359874838	0.84219841
25	0.0227882361334900	0.0226057359874644	0.84260919
29	0.0227882361334896	0.0226057359874220	0.84197301
33	0.0227882361334896	0.0226057359874253	0.84197398

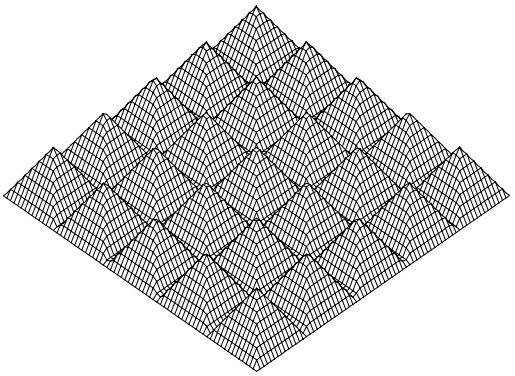

Figure 3.7: A three-dimensional array of square pyramids.

Next, let us consider the problem proposed in [17], that is, a crossed grating of rectangular pyramids with periods $d_1 = 1.50$ and $d_2 = 1$, of height $h = 0.25$, under incident light of wavelength $\lambda = 1.533$ and with incidence angles given as follows: cylindrical angle $\phi = 45°$; azimuthal angle $\theta = 30°$, and polarization with the electric field in the vertical plane $\phi = 45°$. This is an interesting configuration, which contains a three-dimensional obstacle with corners and edges. A schematic representation of the grating is given in Figure 3.7. As we have said, our algorithm requires the boundary of the scatterer to be approximated by a finite Fourier series, thus effectively rounding its edges. For comparison purposes we show, in Figure 3.8, one element of the grating of Figure 3.7 together with its Fourier series approximation with $F = 10$. We can conclude that we have obtained the exact solution for the actual pyramid grating within a given error tolerance when convergence within that tolerance is observed as the number of Fourier modes in the approximation is increased.

As we explained in section 3.3.3, it is necessary here to choose appropriately the truncation parameters F, q_0, and q_1 as well as the order n of the approximation. In the cases below we found that convergence to the actual numerical solution within the error estimates indicated in Table 3.6 is achieved with $F = 5$, $q_0 = q_1 = 20$, and

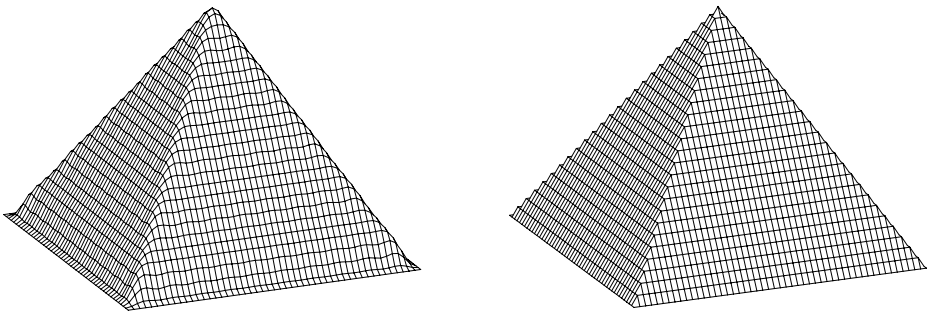

Figure 3.8: An element of the grating of Figure 3.7: (a) Fourier approximation with $F = 10$; (b) exact.

Table 3.6: Efficiencies for the grating of pyramids described in the text: [4/4] Padé approximants.

h	$e_{r,0,0}$	$e_{r,-1,0}$	$e_{t,0,0}$	$e_{t,1,0}$	$e_{t,-1,0}$	$e_{t,0,-1}$	$e_{t,-1,-1}$	ϵ
0.00	0.02525	0.00000	0.97475	0.00000	0.00000	0.00000	0.00000	−1E−16
0.05	0.02500	0.00010	0.97432	0.00012	0.00013	0.00029	0.00004	−2E−12
0.10	0.02425	0.00041	0.97306	0.00049	0.00050	0.00115	0.00015	−8E−10
0.15	0.02304	0.00092	0.97099	0.00107	0.00110	0.00256	0.00032	−2E−08
0.20	0.02143	0.00161	0.96817	0.00185	0.00192	0.00445	0.00056	−2E−07
0.25	0.01951	0.00246	0.96465	0.00280	0.00294	0.00679	0.00086	−1E−06
0.30	0.01737	0.00341	0.96051	0.00388	0.00415	0.00948	0.00120	−6E−06
0.35	0.01511	0.00441	0.95582	0.00506	0.00553	0.01247	0.00157	−2E−05
0.40	0.01284	0.00540	0.95068	0.00631	0.00709	0.01567	0.00196	−5E−05
0.45	0.01064	0.00633	0.94515	0.00758	0.00882	0.01901	0.00237	−1E−04
0.50	0.00858	0.00713	0.93933	0.00885	0.01070	0.02241	0.00278	−2E−04

$n = 9$. Indeed, additional calculations with $F = 10$ and with $q_0 = q_1 = 22$, 24, and 30 result in no changes in the values shown in Table 3.6—exception being made for small changes in the error estimator. This suggests that the solution obtained with $F = 5$ is, within the accuracy shown in Table 3.6, the exact solution to the sharp-edge problem under consideration.

In [17] the authors treated this problem by means of their integral algorithm, and they reported the results of Table 3.7. In addition to results given by the integral method, which is the one the authors recommend, they also presented calculations performed by means of two other solvers based on solution of ordinary differential equations. These differential methods are known to be unstable and generally less competitive than those based on solutions of integral equations [61]. Interestingly, in this particular case one of the differential algorithms produced good results with defect ϵ of order $2 \cdot 10^{-5}$; the other produced $2 \cdot 10^{-3}$. Compare our results in Table 3.6.

Table 3.7: Efficiencies for the grating of pyramids described in the text; values given in reference [17].

h	$e_{r,0,0}$	$e_{r,-1,0}$	$e_{t,0,0}$	$e_{t,1,0}$	$e_{t,-1,0}$	$e_{t,0,-1}$	$e_{t,-1,-1}$	ϵ
0.25	0.01984	0.00254	0.96219	0.00299	0.00303	0.00704	0.00092	1E−03

Table 3.8: Energy and error values for scatterers $\rho = a + \delta\left[\frac{3}{8}\cos(\phi)\sin(\theta)\left(4 - 5\sin^2(\theta)\right)\right]$ (cf. Fig. 3.9).

Padé	δ	Energy	ϵ (Taylor)	ϵ (Padé)
[5/5]	0.5	1.7853305	2.5E–03	5.3E–07
[5/5]	1.0	2.0208911	9.0E–01	1.6E–04

Finally, we present some of the results we have obtained on problems of scattering by acoustically soft bounded bodies [13]. For these applications the scatterers were realized as (large) perturbations of a sphere of radius a: in spherical coordinates (ρ, θ, ϕ) (θ = azimuthal angle and ϕ = polar angle) their boundaries are given by

$$\Gamma_\delta = \{(\rho, \theta, \phi) \,:\, \rho = a + \delta f(\theta, \phi)\}\,,$$

where f is an arbitrary function of (θ, ϕ) and δ is the perturbation parameter.

In Table 3.8 we present calculations and error estimates for the field reflected by the heart-shaped scatterer of Figure 3.9 and related variations of it. The parameter ϵ in the table is, as in the previous applications, a convenient error estimator given by the defect in the energy balance. The values of the fields were obtained by means of direct summation of the Taylor series of the fields (Taylor) and by means of Padé approximation (Padé). As is apparent from an examination of the error estimates in Table 3.8, very accurate results have been obtained in these cases through Padé approximation, providing a substantial improvement over direct summation of the Taylor series (which, in fact, *diverges* for $\delta = 1.0$).

3.5.3 Eigenvalue Calculations

The scattering algorithms described above are based on our results on the analytic dependence of the fields and their boundary values upon boundary variations. As we have explained (section 3.3), these results, in turn, rely heavily on the uniqueness of solutions to the scattering problem, which allows for the inversion of the differential operators within suitable spaces of holomorphic functions. A number of important problems in electromagnetics and acoustics, on the other hand, give rise to models for which this uniqueness property does not hold. This is the case, for instance, in the study of cavities and waveguides (see, e.g., [20, 29] and the references cited there), where *eigenvalue problems* naturally arise. For example, the determination of these eigenvalues and eigenfunctions plays a central role in the assessment of the

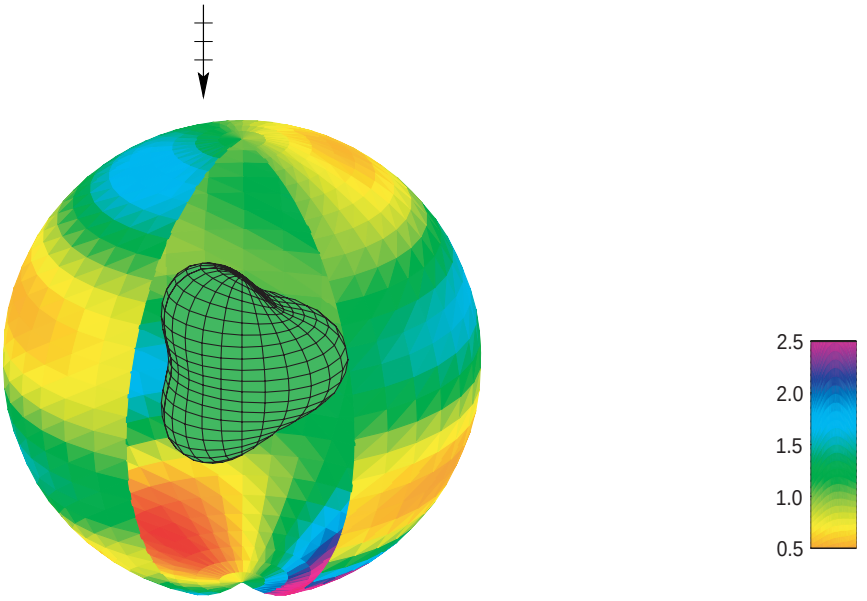

Figure 3.9: An acoustically soft scatterer with boundary $\rho = a+\delta\left[\frac{3}{8}\cos(\phi)\sin(\theta)\times\left(4-5\sin^2(\theta)\right)\right]$: far field for $ka = 1$ and $\delta = 0.5$, *normalized* to that produced by the sphere $\rho = a$.

quality ("Q-factor") of resonators for use in lasers and other optical systems [15, 34]. Thus, substantial literature has been devoted to the shape dependence of Q-factors, that includes the proposition of a number of numerical approaches for their estimation (see, e.g., [63] for an FDTD calculation and [43, 45] for results of raytracing).

The general observation that small to moderate shape changes can have dramatic effects on the properties of conservative and leaky cavities (see, e.g., [19] for a recent experiment) has generated considerable interest in the development of perturbation methods that might shed light on this process [15, 28, 31, 33]. All the work to date, however, has resulted only in low (first- and second-) order theories, and thus it is restricted to very small perturbations. In fact, these results have prompted the suggestion [43] that perturbative methods may be applicable only within this limited range. We know, however, that appropriate uses of analytic function theory can substantially enlarge the domain of applicability of these methods, at least in scattering calculations. And, motivated by these results, we have recently embarked on a project to develop a high-order boundary perturbation theory that will be applicable to the calculation of normal and quasi-normal modes of arbitrarily shaped resonators.

As we had anticipated, the development of such a theory entailed the unraveling of significant new theoretical and algorithmic challenges that were not present in our scattering applications and that certainly do not arise in connection with low-

order approximations. First, on the theoretical side, the issue of analyticity in spatial and perturbation variables (cf. section 3.3) remained to be settled. Indeed, although the analyticity of eigenvalues could be derived from classical results [30, 51], the possibility of choosing corresponding eigenfunctions that are *jointly* analytic in space and parameter variables—so that formal boundary differentiations are permissible—needed to be established. The classical results, however, did prove useful in our effort to demonstrate this latter property of eigenfunctions, as they allowed us to translate the problem to that of uncovering analytic extensions of suitable volume potentials (generated by the appropriate Green's functions).

These theoretical considerations justified, once again, all boundary differentiations and the consequent derivation of appropriate recursive formulas (cf. section 3.3.2). Still, this procedure presented us with yet another unprecedented complication. Indeed, new difficulties arose as we attempted to derive formulas for the continuation of *multiple* eigenvalues of the unperturbed configuration which evolve, upon shape deformation, as separate, *distinct* eigenvalues. Such is the case, for instance, for the simplest case of the Laplace operator on a (two-dimensional) disk. Our theoretical results, on the other hand, guaranteed the existence of an appropriate choice of eigenfunctions so that the problem reduced to finding an efficient process for their identification.

To describe this process, let us consider eigenvalue problems for Laplace's equation in domains with boundaries (3.21). That is, we seek solutions $(u(\vec{x};\delta), k(\delta))$ of

$$\begin{cases} \Delta_x u(\vec{x};\delta) + k(\delta)^2 u(\vec{x};\delta) = 0 & \text{for} \quad \vec{x} \in \Omega_\delta \equiv \{r \le a + \delta f(\theta)\}\,, \\ \qquad \text{and} \qquad\qquad u(\vec{x};\delta) = 0 & \text{for} \quad \vec{x} \in \partial\Omega_\delta. \end{cases}$$

Then, writing

$$u(\vec{x};\delta) = \sum_{k\ge 0} u_k(\vec{x})\delta^k \quad \text{and} \quad k(\delta)^2 = \sum_{k\ge 0} q_k \delta^k,$$

we find the recursive relations

$$\begin{cases} \Delta u_n(r,\theta) + q_0 u_n(r,\theta) = -\sum_{p=0}^{n-1} q_{n-p} u_p(r,\theta) & \text{for} \quad r \le a\,, \\ \qquad \text{and} \qquad u_n(a,\theta) = -\sum_{m=0}^{n-1} \frac{f(\theta)^{n-m}}{(n-m)!} \frac{\partial^{n-m} u_m}{\partial r^{n-m}}(a,\theta). \end{cases} \tag{3.28}$$

The function u_0 corresponds, of course, to an eigenfunction of the Laplacian in the disk Ω_0 and is therefore given by

$$u_0(r,\theta) = \alpha_0 J_M(q_0^{1/2} r) e^{iM\theta} + \beta_0 J_M(q_0^{1/2} r) e^{-iM\theta}, \quad \alpha_0, \beta_0 \in \mathbb{R}, \tag{3.29}$$

where J_M denotes the Bessel function of order $M \ge 0$, and the unperturbed eigenvalue q_0 satisfies

$$J_M(q_0^{1/2} a) = 0.$$

Note that the constants α_0, β_0 in (3.29) are arbitrary (any linear combination provides an eigenfunction in Ω_0) since q_0 has multiplicity 2. However, upon boundary deformations this double eigenvalue will, in general, "split" into two simple ones, each having only a one-dimensional family of associated eigenfunctions. The requirement of analyticity (or even continuity) in δ of these eigenfunctions will thus force a very particular choice of the constants α_0, β_0. As we shall see below, however, this choice may not be apparent until several Taylor coefficients in the expansion for $(u(\cdot,\delta), k(\delta))$ have been derived, as the aforementioned splitting may occur at any order in δ, depending on the perturbation function $f(\theta)$. For this reason, our algorithm to find the coefficients $(u_n(\cdot), q_n)$ in (3.28) proceeds in several steps, which we now discuss briefly.

Step 1. Assume

$$u_0(r,\theta) = J_M(q_0^{1/2} r) e^{iM\theta}. \tag{3.30}$$

Note that, as already stated, this assumption will generally be inconsistent with the desired analytic dependence of eigenfunctions on the perturbation parameter and will therefore have to be reconsidered at a latter stage of the algorithm (see Step 5). Moreover, even if we assume u_0 to have this form, the question arises as to how to expand the successive derivatives u_n. A possible choice for basis functions is the actual eigenfunctions of the unperturbed geometry. However, such a choice would result in infinite series representations, and we therefore choose instead to define functions

$$\psi_{k,l}(r) = \frac{r^k}{(4q_0)^{k/2} k!} J_{l+k}(q_0^{1/2} r) \quad \text{and} \quad \phi_{k,l}(r,\theta) = \psi_{k,|l|}(r) e^{il\theta}.$$

These functions are characterized by

$$P_l(\psi_{k,l}) = \psi_{k-1,l} \quad \text{and} \quad \mathcal{L}(\phi_{k,l}) = \phi_{k-1,l}, \tag{3.31}$$

where

$$P_l(\cdot) = \partial_r^2 + \frac{1}{r}\partial_r + \left(q_0 - \frac{l^2}{r^2}\right) \quad \text{and} \quad \mathcal{L}(\cdot) = \Delta + q_0.$$

And, if $f(\theta)$ has a Fourier series expansion

$$f(\theta) = \sum_{l=-F}^{F} C_{1,l} e^{il\theta},$$

we will seek u_n of the form

$$u_n(r,\theta) = \sum_{\substack{0\le k\le n \\ M-(n-k)F \le l \le M-(n-k)F}} d_{k,l}^n \, \phi_{k,l}(r,\theta). \tag{3.32}$$

Step 2. Find q_n. Multiplying the first equation in (3.28) by $\overline{u_0}$ and integrating on $\{r \le a\}$ we find that

$$q_n = \frac{1}{A^0_{1,|M|}} \left[- \sum_{\substack{1\le p\le n-1 \\ 0\le k\le p}} q_{n-p} d^p_{k,M} A^0_{k+1,|M|} \right.$$
$$\left. + \sum_{\substack{0\le m\le n-1 \\ 0\le k\le m \\ M-\min(m-k,n-m)F\le s\le M+\min(m-k,n-m)F}} C_{n-m,M-s} d^m_{k,s} A^{n-m}_{k,|s|} \right],$$

where

$$A^m_{n,l} = \partial^m_r \psi_{n,l}\Big|_{r=a} \quad \text{and} \quad \frac{f(\theta)^n}{n!} = \sum_{l=-nF}^{nF} C_{n,l} e^{il\theta}.$$

Step 3. Find $d^n_{k,l}$ for $1 \le k \le n$ (all except $k = 0$). For this, we use the differential equation for u_n (cf. (3.28)) and the properties (3.31), which imply that

$$\mathcal{L}(u_n) = \sum_{k,l} d^n_{k,l}\, \phi_{k-1,l} = -\sum_p q_{n-p} \sum_k d^p_{k,l}\, \phi_{k,l}$$

and therefore

$$d^n_{k,l} = -\sum_{p=k-1}^{n-1} q_{n-p}\, d^p_{k-1,l}.$$

Step 4. Find $d^n_{0,l}$ and *check for eigenvalue "splitting."* For this, let $v_n = \sum_l d^n_{0,l}\, \phi_{0,l}$ and recall that $\phi_{0,l}(r,\theta) = J_l(q_0^{1/2} r) e^{il\theta}$ solves $(\Delta + q_0)\phi_{0,l} = 0$. Then, from (3.28), (3.32),

$$\begin{cases} \Delta v_n(r,\theta) + q_0 v_n(r,\theta) = 0 \quad \text{for} \quad r \le a\,, \\ \\ v_n(a,\theta) = -\sum_{m=0}^{n-1} \frac{f(\theta)^{n-m}}{(n-m)!}\, \partial_r^{n-m} u_m(a,\theta) - \sum_{\substack{1\le k\le n \\ l}} d^n_{k,l}\, \phi_{k,l}(a,\theta). \end{cases}$$

Thus, if B^n_l denotes the lth Fourier coefficient of the boundary values $v_n(a,\theta)$,

$$v_n(a,\theta) = \sum_l B^n_l e^{il\theta}, \tag{3.33}$$

then the solution takes the form

$$v_n(r,\theta) = \sum_l \frac{B^n_l}{J_{|l|}(q_0^{1/2} a)}\, J_l(q_0^{1/2} r)\, e^{il\theta}. \tag{3.34}$$

Now, the choice of q_n (cf. Step 2) guarantees that the coefficient B_M^n of the (resonant) mode $l = M$ in (3.33) vanishes (recall $J_M(q_0^{1/2}a) = 0$). However, the coefficient B_{-M}^n may or may not vanish. And, in fact, it can be shown that

$$\text{the eigenvalue "splits"} \iff B_{-M}^n \neq 0.$$

Therefore, the procedure follows different paths depending on the value B_{-M}^n. If $B_{-M}^n = 0$, then we may indeed define v_n as in (3.34) and continue: replace $n \to n+1$ and go back to Step 2. Otherwise, if $B_{-M}^n \neq 0$ we proceed to the next step.

Step 5. "Recalculate" (the correct value of) q_n and choose appropriate eigenfunctions to order 0. As we said, once the splitting has been identified it needs to be accounted for by an appropriate choice of the constants α_0 and β_0 in (3.29) and the determination of coefficients q_n^+ and q_n^- corresponding to each of the two distinct eigenvalues, which have been found (cf. Step 4) to split at order n (i.e., $q_k^+ = q_k^- = q_k$ for $1 \le k \le n-1$). To this end, we first note that if we begin the procedure, in Step 1, with u_0 in (3.30) replaced by

$$u_0^1 = \alpha_0 u_0 + \beta_0 \overline{u_0},$$

we get that the corresponding higher-order coefficients u_k will be given by

$$u_k^1 = \alpha_0 u_k + \beta_0 \overline{u_k} \qquad (1 \le k \le n-1),$$

which satisfy

$$\begin{cases} \Delta u_k^1(r,\theta) + q_0 u_k^1(r,\theta) = -\sum_{p=0}^{k-1} q_{k-p} u_k^1(r,\theta) & \text{for} \quad r \le a \\ \\ \quad \text{and} \qquad u_k^1(a,\theta) = -\sum_{m=0}^{k-1} \frac{f(\theta)^{k-m}}{(k-m)!} \frac{\partial^{k-m} u_m^1}{\partial r^{k-m}}(a,\theta). \end{cases}$$

To find q_n, α_0, and β_0, we multiply the first equation above for $k = n$ by $(\frac{u_0}{u_0})$ and integrate in $\{r \le a\}$. After some straightforward calculations we find that

$$q_n^\pm = q_n \pm \frac{|B_{-M}^n|}{\psi_{1,|M|}(a)}, \qquad \alpha_0^\pm = \mp |B_{-M}^n| \qquad \text{and} \qquad \beta_0^\pm = B_{-M}^n, \tag{3.35}$$

where the superscripts $\pm$ differentiate the two (simple) eigenvalues. Thus, we define

$$u_k^{1,\pm} = \alpha_0^\pm u_k + \beta_0^\pm \overline{u_k} \quad \text{for } 0 \le k \le n-1,$$

and now $u_n^{1,\pm}$ can be computed as in Steps 3 and 4, since the choices in (3.35) guarantee that the new $B_{\pm M}^n$ vanish.

Step 6. Calculate $q_{n+1+\nu}$ and choose appropriate eigenfunctions to order $1+\nu$ for each $\nu \ge 0$ (iterate in ν). For this, assume that for a fixed integer $\nu \ge 0$ we have calculated

$$\left\{u_k^{\nu+1,\pm}\right\}_{k=0}^{n+\nu} \quad \text{and} \quad \left\{q_k^\pm\right\}_{k=0}^{n+\nu} \qquad (q_k^\pm = q_k \text{ for } k = 0, \dots, n-1).$$

We want to define $q_{n+\nu+1}^\pm$ and new corrections $\left\{u_k^{\nu+2,\pm}\right\}_{k=1}^{n+\nu+1}$, where

$$u_k^{\nu+2,\pm} = u_k^{\nu+1,\pm} \quad \text{for} \quad k = 0, \dots, \nu.$$

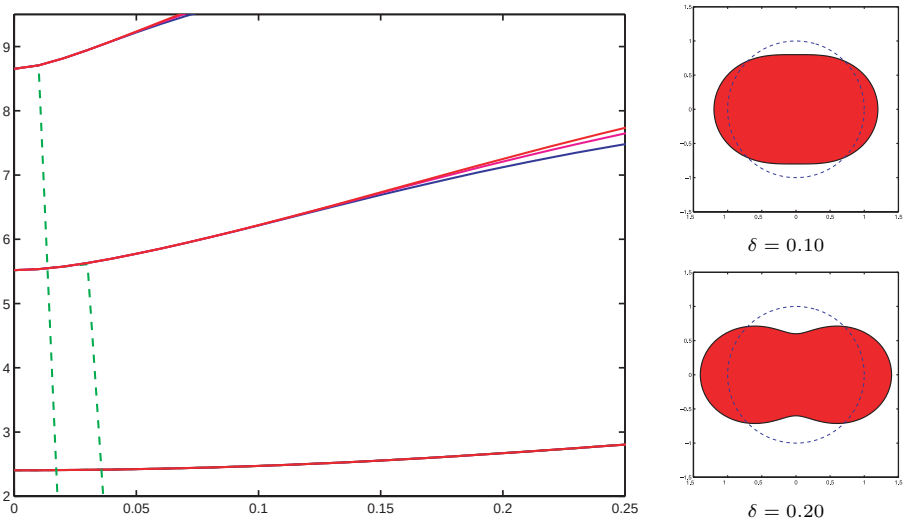

Figure 3.10: Continuation of three zeros of J_0 as eigenfrequencies for perturbations with $f(\theta) = 2\cos(2\theta)$. *No splitting.* Dashed green: Taylor series (order 28); solid blue: Padé [10/10]; solid magenta: Padé [12/12]; solid red: Padé [14/14]. Inset: domains $r = 1 + \delta f(\theta)$ for $\delta = 0.10$ and $\delta = 0.20$.

For instance, if $\nu = 0$, we want to define $q_{n+1}^{\pm}$ and corrections $\{u_k^{2,\pm}\}_{k=0}^{n+1}$; however, $u_0^{2,\pm} = u_0^{1,\pm}$ has already been appropriately chosen in the previous step. We shall then look for solutions $u_k^{\nu+2,\pm}$ of the form

$$\begin{aligned} u_k^{\nu+2,\pm} &= u_k^{\nu+1,\pm} && \text{for } k = 0, \ldots, \nu, \\ u_k^{\nu+2,\pm} &= u_k^{\nu+1,\pm} + \alpha_{\nu+1}^{\pm} u_{k-\nu-1} + \beta_{\nu+1}^{\pm} \overline{u}_{k-\nu-1} && \text{for } k = \nu+1, \ldots, n+\nu, \end{aligned}$$

where the u_m, $0 \le m \le n-1$, are those that were originally found (Steps 1–4). As before (Step 5), from the orthogonality conditions it is possible to find the values of $q_{n+1+\nu}^{\pm}$, $\alpha_{\nu+1}^{\pm}$, and $\beta_{\nu+1}^{\pm}$. And, finally, $u_{n+\nu+1}^{\nu+2,\pm}$ can be determined as in Steps 3 and 4.

We have implemented the above algorithm and have conducted experiments for a variety of perturbations $f(\theta)$. Figures 3.10–3.13 depict the results of our codes in cases were no splitting occurs and were the eigenvalues separate at orders $n = 1$, 2, and 4, respectively. We conclude with Table 3.9 where we record the outcome of convergence studies for the case of first-order splitting (Figure 3.11). These results show that very accurate approximations can be achieved for substantial deformations which may be well beyond the disk of convergence of the Taylor series.

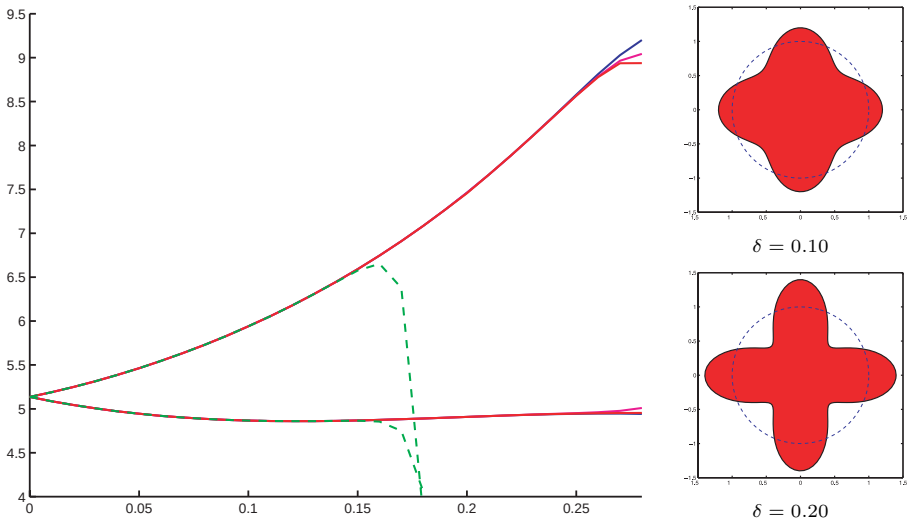

Figure 3.11: Continuation of a zero of J_2 as eigenfrequencies for perturbations with $f(\theta) = 2\cos(4\theta)$. *Splitting at order* 1. Dashed green: Taylor series (order 28); solid blue: Padé [10/10]; solid magenta: Padé [12/12]; solid red: Padé [14/14]. Inset: domains $r = 1 + \delta f(\theta)$ for $\delta = 0.10$ and $\delta = 0.20$.

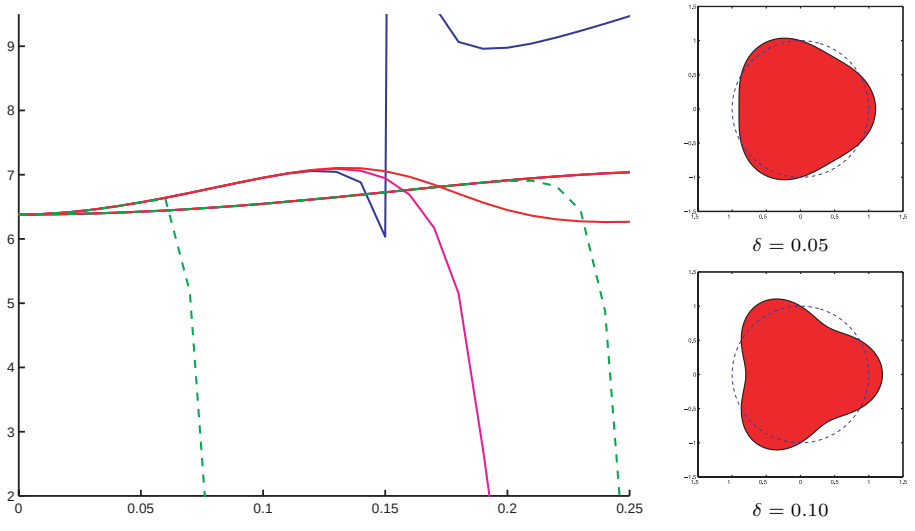

Figure 3.12: Continuation of a zero of J_3 as eigenfrequencies for perturbations with $f(\theta) = 2\cos(3\theta)$. *Splitting at order* 2. Dashed green: Taylor series (order 28); solid blue: Padé [10/10]; solid magenta: Padé [12/12]; solid red: Padé [14/14]. Inset: domains $r = 1 + \delta f(\theta)$ for $\delta = 0.05$ and $\delta = 0.10$.

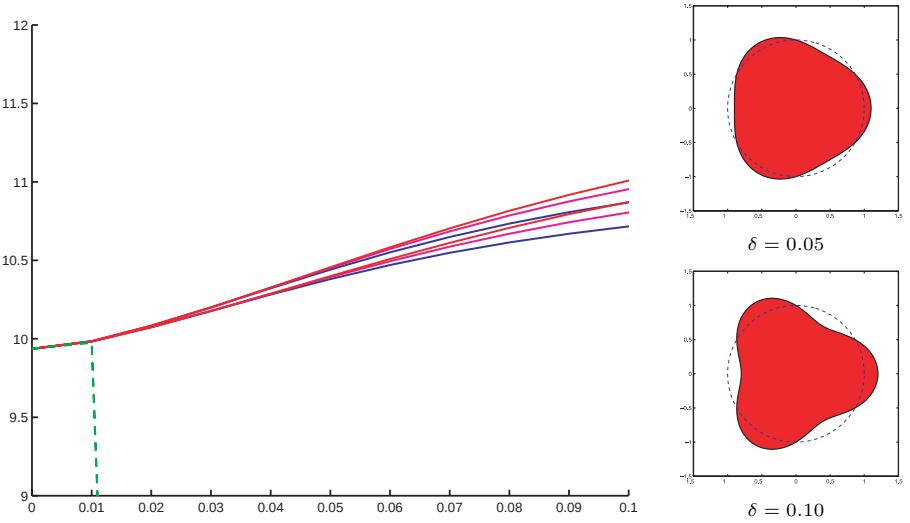

Figure 3.13: Continuation of a zero of J_6 as eigenfrequencies for perturbations with $f(\theta) = 2\cos(3\theta)$. *Splitting at order* 4. Dashed green: Taylor series (order 28); solid blue: Padé [10/10]; solid magenta: Padé [12/12]; solid red: Padé [14/14]. Inset: domains $r = 1 + \delta f(\theta)$ for $\delta = 0.05$ and $\delta = 0.10$.

Table 3.9: Numerical values for the example of Figure 3.11: $f(\theta) = 2\cos(4\theta)$. Continuation of the zero $z = 5.1356223$ of $J_2(z)$.

N	δ	Padé ($[N/2, N/2]$)	Taylor (N)
4	0.10	5.932459814	5.933746721
8	0.10	5.939888161	5.939685615
12	0.10	5.940103147	5.940002737
16	0.10	5.940063852	5.940052067
20	0.10	5.940063913	5.940061333
24	0.10	5.940063912	5.940063302
28	0.10	5.940063912	5.940063758

N	δ	Padé ($[N/2, N/2]$)	Taylor (N)
4	0.20	7.250946252	7.290785243
8	0.20	7.430618958	7.338717672
12	0.20	7.476836436	7.147414978
16	0.20	7.459583127	6.463497406
20	0.20	7.462505263	2.837427216
24	0.20	7.462303523	Diverges

References

[1] G. V. Anand and M. K. George, *Normal mode sound propagation in an ocean with sinusoidal surface waves,* J. Acoust. Soc. Amer., 80 (1986), pp. 238–243.

[2] G. V. Anand and M. K. George, *Normal mode sound propagation in an ocean with random narrow–band surface waves,* J. Acoust. Soc. Amer., 94 (1993), pp. 279–292.

[3] G. A. Baker and P. Graves-Morris, *Padé Approximants,* 2*nd ed.*, Encyclopedia Math. Appl. 59, Cambridge University Press, Cambridge, UK 1996.

[4] J. J. Bowman, T. B. A. Senior, and P. L. E. Uslenghi, *Electromagnetic and acoustic scattering by simple shapes*, Revised Printing, Hemisphere Publishing, New York, 1987.

[5] C. Brezinski, *Procedures for estimating the error in Padé approximation*, Math. Comp., 53 (1965), pp. 639–648.

[6] O. P. Bruno and P. Laurence, *On the MHD equations in a three-dimensional toroidal geometry*, Comm. Pure Appl. Math., 49 (1996), pp. 717–764.

[7] O. P. Bruno and F. Reitich, *Solution of a boundary value problem for Helmholtz equation via variation of the boundary into the complex domain*, Proc. Roy. Soc. Edinburgh, 122A (1992), pp. 317–340.

[8] O. P. Bruno and F. Reitich, *Numerical solution of diffraction problems: A method of variation of boundaries*, J. Opt. Soc. Amer. A, 10 (1993), pp. 1168–1175.

[9] O. P. Bruno and F. Reitich, *Numerical solution of diffraction problems: A method of variation of boundaries* II. *Dielectric gratings, Padé approximants and singularities*, J. Opt. Soc. Amer. A, 10 (1993), pp. 2307–2316.

[10] O. P. Bruno and F. Reitich, *Numerical solution of diffraction problems: A method of variation of boundaries* III. *Doubly periodic gratings*, J. Opt. Soc. Amer. A, 10 (1993), pp. 2551–2562.

[11] O. P. Bruno and F. Reitich, *Approximation of analytic functions: A method of enhanced convergence*, Math. Comp., 63 (1994), pp. 195–213.

[12] O. P. Bruno and F. Reitich, *Calculation of electromagnetic scattering via boundary variations and analytic continuation*, ACES J., 11 (1996), pp. 17–31.

[13] O. P. Bruno and F. Reitich, *Boundary-variation solutions for bounded-obstacle scattering in three dimensions*, J. Acoust. Soc. Amer., 104 (1998), pp. 2579–2583.

[14] A. P. Calderón, *Cauchy integrals on Lipschitz curves and related operators*, Proc. Nat. Acad. Sci. USA, 75 (1977), pp. 1324–1327.

[15] R. K. Chang and A. J. Campillo, *Optical Processes in Microcavities*, World Scientific, Singapore, 1996.

[16] R. R. Coifman, A. MacIntosh, and Y. Meyer, *L'integrale de Cauchy définit un opérateur borné sur L^2 pour les courbes Lipschitziennes*, Ann. of Math., 116 (1982), pp. 361–387.

[17] G. H. Derrick, R. C. McPhedran, D. Maystre, and M. Nevière, *Crossed gratings: A theory and its applications*, in Electromagnetic Theory of Gratings, R. Petit, ed., Springer-Verlag, Berlin, 1980, pp. 227–275.

[18] D. C. Dobson and J. A. Cox, *An integral equation method for biperiodic diffraction structures*, in Proc. SPIE 1545, Bellingham, WA, 1991, pp. 106–113.

[19] C. Gmachl, F. Carpasso, E. E. Narimanov, J. U. Nöckel, A. D. Stone, J. Faist, D. L. Sivco, and A. Y. Cho, *High-power directional emission from microlasers with chaotic resonators*, Science, 280 (1998), pp. 1556–1564.

[20] G. Goubau, *Electromagnetic Waveguides and Cavities*, Pergamon Press, London, 1961.

[21] P. Graves-Morris, *The numerical calculation of Padé approximants*, in Lecture Notes in Math. 765, L. Wuytack, ed., Springer-Verlag, Berlin, 1979, pp. 231–245.

[22] J. J. Greffet, *Scattering of electromagnetic waves by rough dielectric surfaces*, Phys. Rev. B, 37 (1988), pp. 6436–6441.

[23] J. J. Greffet, C. Baylard and P. Versaevel, *Diffraction of electromagnetic waves by crossed gratings: A series solution*, Opt. Lett., 17 (1992), pp. 1740–1742.

[24] J. J. Greffet and Z. Maassarani, *Scattering of electromagnetic waves by a grating: A numerical evaluation of the iterative–series solution*, J. Opt. Soc. Amer. A, 7 (1990), pp. 1483–1493.

[25] E. Y. Harper and F. M. Labianca, *Perturbation theory for scattering of sound from a point source by a moving rough surface in the presence of refraction*, J. Acoust. Soc. Amer., 57 (1975), pp. 1044–1051.

[26] E. Y. Harper and F. M. Labianca, *Scattering of sound from a point source by a rough surface progressing over an isovelocity ocean*, J. Acoust. Soc. Amer., 58 (1975), pp. 349–364.

[27] D. R. Jackson, D. P. Winebrenner, and A. Ishimaru, *Comparison of perturbation theories for rough-surface scattering*, J. Acoust. Soc. Amer., 83 (1988), pp. 961–969.

[28] M. S. Janaki and B. Dasgupta, *Eigenmodes in a toroidal cavity of elliptic cross section*, IEEE Trans. Microwave Theory Tech., 44 (1996), pp. 1147–1150.

[29] D. S. Jones, *The theory of electromagnetism*, MacMillan, New York, 1964.

[30] T. Kato, *Perturbation theory for linear operators, 2nd ed.*, Springer-Verlag, Berlin, 1980.

[31] G. C. Kokkorakis and J. A. Roumeliotis, *Electromagnetic eigenfrequencies in a spheroidal cavity*, J. Electromagnetic Waves Appl., 11 (1997), pp. 279–292.

[32] W. A. Kuperman and F. Ingenito, *Attenuation of the coherent component of sound propagating in shallow water with rough boundaries*, J. Acoust. Soc. Amer., 61 (1977), pp. 1178–1187.

[33] H. M. Lai, P. T. Leung, K. Young, P. W. Barber, and S. C. Hill, *Time-independent perturbation for leaking electromagnetic modes in open systems with application to resonances in microdroplets*, Phys. Rev. A, 41 (1990), pp. 5187–5198.

[34] L. Levi, *Applied Optics*, Wiley, New York, 1968.

[35] Y. Liu, S. J. Frasier, and R. E. McIntosh, *Measurement and classification of low-grazing-angle radar sea spikes*, IEEE Trans. Antennas and Propagation, 46 (1998), pp. 27–40.

[36] C. Lopez, F. J. Yndurain, and N. Garcia, *Iterative series for calculating the scattering of waves from hard corrugated surfaces*, Phys. Rev. B, 18 (1978), pp. 970–972.

[37] A. A. Maradudin, *Iterative solutions for electromagnetic scattering by gratings*, J. Opt. Soc. Amer., 73 (1983), pp. 759–764.

[38] D. Maystre, *Rigorous vector theories of diffraction gratings*, in Progress in Optics, E. Wolf, ed., North Holland, Amsterdam, 1984, pp. 3–67.

[39] D. Maystre and M. Nevière, *Electromagnetic theory of crossed gratings*, J. Optics, 9 (1978), pp. 301–306.

[40] D. Maystre, M. Nevière, and R. Petit, *Experimental verifications and applications of the theory*, in Electromagnetic Theory of Gratings, R. Petit, ed., Springer-Verlag, Berlin, 1980, pp. 159–223.

[41] R. C. McPhedran, G. H. Derrick, and L. C. Botten, *Theory of crossed gratings*, in Electromagnetic Theory of Gratings, R. Petit, ed., Springer-Verlag, Berlin, 1980, pp. 227–275.

[42] W. C. Meecham, *On the use of the Kirchoff approximation for the solution of reflection problems*, J. Rational Mech. Anal., 5 (1956), pp. 323–334.

[43] A. Mekis, J. U. Nöckel, G. Chen, A. D. Stone, and R. K. Chang, *Ray chaos and Q spoiling of lasing droplets*, Phys. Rev. Lett., 75 (1995), pp. 2682–2685.

[44] A. H. Nayfeh and O. R. Asfar, *Parallel-plate waveguide with sinusoidally perturbed boundaries*, J. Appl. Phys., 45 (1974), pp. 4797–4800.

[45] J. U. Nökel, A. D. Stone, and R. K. Chang, *Q spoiling and directionality in deformed ring cavities*, Optics Letters, 19 (1994), pp. 1693–1695.

[46] J. Pavageau and J. Bousquet, *Diffraction par un réseau conducteur nouvelle méthode de résolution*, Optica Acta, 17 (1970), pp. 469–478.

[47] W. H. Peake, *Theory of radar return from terrain*, IRE Nat'l Conv., 7 (1959), pp. 27–41.

[48] R. Petit, *A tutorial introduction*, in Electromagnetic Theory of Gratings, R. Petit, ed., Springer-Verlag, Berlin, 1980, pp. 1–52.

[49] R. Petit and M. Cadilhac, *Sur la diffraction d'une onde plane par un réseau infinitement conducteur*, C. R. Acad. Sci. Paris Sér. B, 262 (1966), pp. 468–471.

[50] Lord Rayleigh, *The Theory of Sound*, Vol. 2, Dover, New York, 1945.

[51] F. Rellich, *Perturbation Theory of Eigenvalue Problems*, Gordon and Breach Science Publishers, New York, 1969.

[52] S. O. Rice, *Reflection of electromagnetic waves from slightly rough surfaces*, Comm. Pure Appl. Math., 4 (1951), pp. 351–378.

[53] J. Roginsky, *Derivation of closed-form expressions for the T matrices of Rayleigh–Rice and extinction-theorem perturbation theories*, J. Acoust. Soc. Amer., 90 (1991), pp. 1130–1137.

[54] R. E. Scraton, *A note on the summation of divergent power series*, Proc. Cambridge Philos. Soc., 66 (1969), pp. 109–114.

[55] A. Sei, O. Bruno, and M. Caponi, *Study of polarization dependent scattering anomalies with applications to oceanic scattering*, Radio Sci., 34 (1999), pp. 385–411.

[56] N. C. Skaropoulos and D. P. Chrissoulidis, *General perturbative solution to wave scattering from a soft random cylindrical surface*, J. Acoust. Soc. Amer., 106 (1999), pp. 596–604.

[57] D. Talbot, J. B. Titchener, and J. R. Willis, *The reflection of electromagnetic waves from very rough interfaces*, Wave Motion, 12 (1990), pp. 245–260.

[58] J. L. Uretsky, *The scattering of plane waves from periodic surfaces*, Ann. Phys., 33 (1965), pp. 400–427.

[59] G. R. Valenzuela, *Theories for the interaction of electromagnetic and oceanic waves—A review*, Boundary-Layer Meteor., 13 (1978), pp. 61–85.

[60] P. M. Van den Berg, *Diffraction theory of a reflection grating*, Appl. Sci. Res., 24 (1971), pp. 261–293.

[61] P. Vincent, *Differential Methods*, in Electromagnetic Theory of Gratings, R. Petit, ed., Springer-Verlag, Berlin, 1980, pp. 101–121.

[62] J. R. Wait, *Perturbation analysis for reflection from two-dimensional periodic sea waves*, Radio Sci., 6 (1971), pp. 387–391.

[63] C. Wang, B.-Q. Gao, and C.-P. Deng, *Accurate study of Q-factor of resonator by a finite-difference time-domain method*, IEEE Trans. Microwave Theory and Techniques, 43 (1995), pp. 1524–1529.

[64] A. Wirgin, *Scattering from hard and soft corrugated surfaces: Iterative corrections to the Kirchhoff approximation through the extinction theorem*, J. Acoust. Soc. Amer., 85 (1989), pp. 670–679.